




ORIGINAL RESEARCH

Open Access



A fast spectral recovery does not necessarily indicate post-fire forest recovery

Joe V. Celebrezze^{1*} , Madeline C. Franz¹, Robert A. Andrus¹, Amanda T. Stahl¹, Michelle Steen-Adams² and Arjan J. H. Meddens¹

Abstract

Background Climate change has increased wildfire activity in the western USA and limited the capacity for forests to recover post-fire, especially in areas burned at high severity. Land managers urgently need a better understanding of the spatiotemporal variability in natural post-fire forest recovery to plan and implement active recovery projects. In burned areas, post-fire “spectral recovery”, determined by examining the trajectory of multispectral indices (e.g., normalized burn ratio) over time, generally corresponds with recovery of multiple post-fire vegetation types, including trees and shrubs. Field data are essential for deciphering the vegetation types reflected by spectral recovery, yet few studies validate spectral recovery metrics with field data or incorporate spectral recovery into spatial models of post-fire vegetation recovery. We investigated relationships between spectral recovery and field measurements of post-fire recovery (16 to 27 years post-fire) from 99 plots in mixed conifer forests of the Blue Mountains, USA. Additionally, using generalized linear mixed effects models, we assessed the relative capacities of multispectral, climatic, and topographic data to predict field measurements of post-fire recovery.

Results We found that a fast spectral recovery did not necessarily coincide with field measurements of forest recovery (e.g., density of regenerating seedlings, saplings, and young trees and % juvenile conifer cover). Instead, fast spectral recovery often coincided with increases in % shrub cover. We primarily attributed this relationship to the response of snowbrush ceanothus, an evergreen shrub that vigorously resprouts post-fire. However, in non-trailing edge forests—where it was cooler and wetter and fast-growing conifers were more common—rapid spectral recovery coincided with both increases in % shrub cover and forest recovery. Otherwise, spectral recovery showed potential to identify transitions to grasslands, as grass-dominated sites showcased distinctly slow spectral trajectories. Lastly, field measurements of post-fire forest recovery were best predicted when including post-fire climate and multispectral data in predictive models.

Conclusions Despite a disconnect between a fast spectral recovery and forest recovery, our results suggest that including multispectral data improved models predicting the likelihood of post-fire forest recovery. Improving predictive models would aid land managers in identifying sites to implement active reforestation projects.

Keywords Blue Mountains, Conifer forests, High severity wildfire, Normalized burn ratio, Post-fire forest recovery, Spectral recovery, Trailing edge forests

*Correspondence:

Joe V. Celebrezze

joseph.celebrezze@wsu.edu

Full list of author information is available at the end of the article



© The Author(s) 2024. **Open Access** This article is licensed under a Creative Commons Attribution 4.0 International License, which permits use, sharing, adaptation, distribution and reproduction in any medium or format, as long as you give appropriate credit to the original author(s) and the source, provide a link to the Creative Commons licence, and indicate if changes were made. The images or other third party material in this article are included in the article's Creative Commons licence, unless indicated otherwise in a credit line to the material. If material is not included in the article's Creative Commons licence and your intended use is not permitted by statutory regulation or exceeds the permitted use, you will need to obtain permission directly from the copyright holder. To view a copy of this licence, visit <http://creativecommons.org/licenses/by/4.0/>.

Resumen

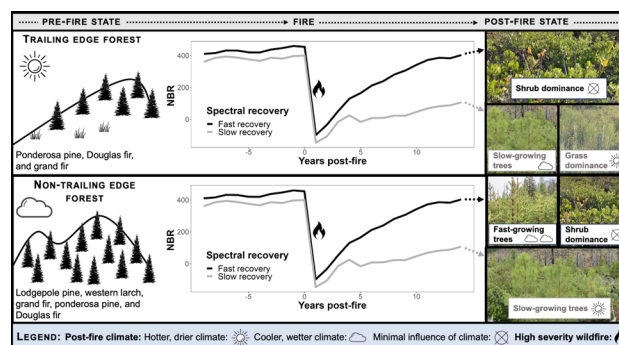
Antecedentes El Cambio Climático ha incrementado la actividad de los incendios en el oeste de los EEUU y limitado la capacidad de los bosques para recuperarse en el post fuego, especialmente en áreas quemadas a alta severidad. Los manejadores de tierras necesitan urgentemente de una mejor comprensión de la variabilidad espacio-temporal en la recuperación natural post fuego, para planear e implementar proyectos activos de recuperación. En áreas quemadas, la “recuperación espectral” post fuego, determinada mediante el examen de la trayectoria de índices multi-espectrales (i.e. relación normalizada de quema, NBR) en el tiempo, generalmente se corresponde con la recuperación de múltiples tipos de vegetación, incluyendo árboles y arbustos. Los datos de campo son esenciales para descifrar los tipos de vegetación reflejados por la recuperación espectral, aunque pocos estudios han validado las medidas de recuperación espectral con datos de campo, o han incorporado la recuperación espectral en modelos espaciales de recuperación de la vegetación en el post fuego. Investigamos las relaciones entre la recuperación espectral y mediciones a campo en la recuperación post fuego (16 a 27 años post fuego), en 99 parcelas en bosques mixtos de las Montañas Azules en los EEUU. Adicionalmente, usando modelos generalizados de efectos lineares mixtos, determinamos las capacidades relativas de los datos espectrales, climáticos, y topográficos para predecir las mediciones de campo en la recuperación post fuego.

Resultados Encontramos que una rápida recuperación espectral no necesariamente coincide con las mediciones de campo sobre recuperación de la vegetación del bosque (i.e. densidad en la regeneración de plántulas, brinzales, y árboles juveniles, y en el porcentaje de cobertura de coníferas jóvenes). En cambio, encontramos que una rápida recuperación espectral frecuentemente coincide con incrementos en el porcentaje de cobertura de arbustos. Atribuimos primariamente esta relación a la respuesta del snowbrush ceanothus, un arbusto siempreverde que rebrota vigorosamente luego de incendios. Desde luego, en áreas al interior de los bordes del bosque, donde el mismo es más frío y húmedo y las coníferas de rápido crecimiento son más comunes, la rápida recuperación espectral coincide tanto con el incremento en el porcentaje de los arbustos como con el del bosque. De todas maneras, la recuperación espectral mostró potencial para identificar transiciones hacia pastizales, dado que los sitios dominados por pastos muestran bajas trayectorias espectrales. Por último, las mediciones a campo sobre la recuperación de la vegetación fueron mejor predichas cuando se incluyeron en ellas el clima post fuego y datos multiespectrales en modelos predictivos.

Conclusiones A pesar de las desconexiones entre las recuperaciones espectrales rápidas y la recuperación del bosque, nuestros resultados sugieren que la inclusión de datos multiespectrales mejora los modelos que predicen la probabilidad de la recuperación del bosque en el post fuego. El mejoramiento de los modelos predictivos podría ayudar a los manejadores de tierras a identificar sitios para implementar proyectos de reforestación activos.

Graphical Abstract

Photo credit: J. Celebrezze



Background

Wildfire frequency and severity have increased over recent decades (Williams and Abatzoglou 2016; Parks

and Abatzoglou 2020), and this trend is expected to intensify with climate change (Abatzoglou and Williams 2016; Coop et al. 2020) heightening the risk of mortality

for trees and shrubs (Enright et al. 2015). For temperate conifer forests in the western USA, climate-change-driven increases in temperature and aridity and close to a century of fire exclusion (Hessburg et al. 2015) have altered historical fire regimes and subsequently impacted the capacity of forests to recover post-fire (Parks et al. 2018; Hagmann et al. 2021). Because forests are economically important (Pearce 2001) and provide key benefits to humans and ecosystems—supporting pollinators, carbon and water cycles, soil formation, and prevention of invasive species (Thompson et al. 2011)—concerns surrounding diminished forest resilience are mounting. In response, there have been changes in frameworks and policy informing land management in the USA. The Resist-Accept-Direct (RAD) framework emerged to inform climate-adaptive land management in the context of changing ecosystems (Schuurman et al. 2022; Rodman et al. 2022), while the Repairing Existing Public Land by Adding Necessary Trees (REPLANT) Act of 2021 increased annual investments towards reforestation projects. In the context of post-fire forest recovery, effective implementation of such innovative frameworks and policies will require an improved ecological understanding of vegetation dynamics in response to climate change and altered fire regimes. Furthermore, with limited resources and ever-expanding demands on agency capacity (Timberlake and Schultz 2019), it is imperative for natural resource managers to identify where to apply active post-fire recovery projects.

In mixed conifer forests, post-fire recovery outcomes can vary widely based on burn severity, species composition, climate, and topography. Accordingly, when identifying priority sites for active post-fire management projects, it is essential to account for the variability of post-fire recovery outcomes and understand patterns of natural post-fire conifer recovery. Following low to moderate severity wildfires (i.e., less than 70% tree mortality), remaining live seedling trees increase the probability for post-fire conifer recovery (Davis et al. 2023). In contrast, following high severity wildfires, which cause higher rates of tree mortality, live seed sources are relatively distant, thus limiting the likelihood of natural forest recovery (Chambers et al. 2016). As a result, reforestation efforts are often prioritized in areas impacted by high severity wildfire where natural forest recovery is less likely and vegetation transition to grasslands is more likely (Davis et al. 2023). Although burn severity has profound effects on post-fire recovery outcomes, high severity wildfire can have contrasting effects on different forest types. Dry mixed conifer forests are more likely classified as the trailing edge of forests where it is warmer, drier, the cumulative water deficit (CWD) is higher (Parks et al. 2019), and seedling establishment is less likely (Kemp

et al. 2019; Davis et al. 2019). Trailing edge forests, especially if burned at a high severity, have a decreased capacity to recover post-fire (Stevens-Rumann et al. 2018) and an increased risk of conversion to grasslands, shrublands, or open woodlands (Coop et al. 2020). Moreover, in dry mixed conifer forests, ponderosa pine (*Pinus ponderosa* Lawson and C. Lawson), and Douglas-fir (*Pseudotsuga menziesii* (Mirb.) Franco) are typically dominant and post-fire seedling establishment primarily relies on passive seed dispersal from existing seed sources, prolonging forest recovery (Agee 1996). In contrast, moist mixed conifer forests, where lodgepole pine (*Pinus contorta* Douglas ex Loudon) is more common, are less likely to be classified as trailing edge forests and showcase key differences in expected post-fire recovery outcomes. Following a high severity wildfire, lodgepole pine stands exhibit a serotinous response, dispersing seeds en masse leading to abundant seedling establishment (Lotan 1976). This vigorous post-fire response limits the likelihood of grasses and shrubs dominating the landscape and often leads to successful post-fire forest recovery (Boag et al. 2020).

Accounting for complex interactions between burn severity, vegetation type, climate, and topography, researchers have developed field-validated spatial models which utilize several factors to predict when and where post-fire forest recovery may or may not occur (Korb et al. 2019). Primarily, climate metrics such as precipitation, temperature, and vapor pressure deficit (VPD) are associated with seedling establishment (Andrus et al. 2022) and have been used to map probability of post-fire conifer regeneration (Davis et al. 2023). Likewise, higher rates of recovery have been observed at higher elevations (Chambers et al. 2016; Rother and Veblen 2016), where climatic conditions are typically cooler and wetter, and in sites with higher surface soil moisture (Fernández-Guisuraga et al. 2023). Topographic metrics (e.g., heat load index [HLI]; Boag et al. 2020), community composition (White et al. 2023), and prior disturbances such as those associated with fuel treatments (e.g., harvest logging, understory thinning, prescribed burns; Dodge et al. 2019) have all been linked to differences in post-fire vegetation dynamics. Despite encouraging results from predictive models utilizing climatic or topographic data, down-scaled climate data can be limited in spatial resolution and precision (Behnke et al. 2016; Baker et al. 2017). Therefore, predictive models that primarily rely on climate may overlook important microsite differences; thus, land management recommendations based on these models could be overgeneralized or misleading. Multispectral remote sensing data have advantages over climatic data, offering precision while being spatially continuous and available at high spatial resolutions.

Thus, when predicting post-fire recovery, researchers have begun to supplement or supplant climate, topography, and pre-fire vegetation type with multispectral data.

Researchers use multispectral indices such as the normalized burn ratio (NBR) or normalized difference vegetation index (NDVI) to describe “spectral recovery”, the post-fire trajectory of spectral index values as they approach pre-fire norms, when investigating post-fire vegetation recovery (Chuvieco et al. 2020). NBR and NDVI have both been effectively used in spectral recovery studies, when predicting post-fire recovery; however, NBR has been shown to outperform NDVI due to a stronger association with vegetation structure (White et al. 2017; Hislop et al. 2018) and less year-to-year climate variability (Storey et al. 2016). Spectral recovery is commonly used when considering post-fire vegetation dynamics (Pérez-Cabello et al. 2021) in many ecosystems, including boreal forests (White et al. 2017), chaparral (Storey et al. 2016), Mediterranean pine forests (Viana-Soto et al. 2020), ponderosa pine forests, mixed conifer forests, and conifer-oak-chaparral (Meng et al. 2015; Bright et al. 2019). The increasing use of spectral recovery has shown promising results; however, in many instances, spectral recovery has not been validated with field data (but see Fiore et al. 2020; White et al. 2023; Smith-Tripp et al. 2024), raising concerns regarding what spectral recovery represents. This warrants scrutiny, as spectral recovery may be misinterpreted as post-fire forest recovery in ecological contexts where the two have not been explicitly linked.

Our primary research objective was to compare spectral recovery metrics to field measurements of post-fire vegetation dynamics in mixed conifer forests burned at a high severity in the Blue Mountains, USA. We conducted top-down (spectral recovery metrics as input variables) and bottom-up (field measurements as input variables) *k*-means cluster analyses to explore relationships between spectral recovery and post-fire recovery of conifers, shrubs, and grasses. Furthermore, we investigated the relative contributions of multispectral, climatic, and topographic data when predicting field measurements of post-fire vegetation dynamics to test whether supplementing existing predictive models, which primarily rely on climatic and topographic predictors, with multispectral data could lead to improvements in identifying priority sites for active post-fire management. Lastly, we analyzed relationships between climate, spectral recovery, and field measurements of post-fire vegetation dynamics in trailing edge and non-trailing edge sites to isolate patterns in trailing edge forests, where post-fire forest recovery is uncertain, and to test how relationships vary in different ecological contexts.

Methods

Study area

The Blue Mountains ecoregion spans eastern Oregon, areas of southeastern Washington, and western Idaho. The Blue Mountains are influenced by forestry practices, the timber trade, and conversion to rangeland (Soulard 2012; Stine et al. 2014), and much of the ecoregion is federal land—including the Malheur, Ochoco, Umatilla, and Wallowa-Whitman National Forests and designated national wilderness areas. Soils are classified as loamy sand derived from basalt layers, loess deposits, and volcanic ash (including Mazama ash; NRCS 2012). The climate is characterized by hot and dry summers and cool and wet winters. Along the southern and western edges of the mountains (e.g., see Egley, Hash Rock, Wheeler Point fires in Fig. 1 and Table 1), it is typically drier with hotter summers. Additionally, topography drives climatic differences, as there is a wide range in elevation (700 to 3000 m), and it is typically cooler and wetter with increased snowfall at higher elevations and hotter and drier at lower elevations.

Similarly, climate and elevation correspond with tree species composition in the forests of the Blue Mountains. Western juniper (*Juniperus occidentalis* Hook.) woodlands, shrublands, and grasslands are common in the lowest elevation sites, while dry mixed conifer forests composed of ponderosa pine (*Pinus ponderosa*) and Douglas-fir (*Pseudotsuga menziesii*) are dominant at low-to-mid elevation sites with scattered grand fir (*Abies grandis* (Dougl.) Lindl.) and western juniper. Moist mixed conifer forests are dominant at mid-to-high elevations, commonly composed of grand fir and western larch (*Larix occidentalis* Nutt.) intermixing with ponderosa pine and Douglas-fir, while north-facing slopes or cooler upland sites showcase lodgepole pine (*Pinus contorta*), subalpine fir (*Abies lasiocarpa* (Hook.) Nutt.), Engelmann spruce (*Picea engelmanni* Parry ex Engelm.), and whitebark pine (*Pinus albicaulus* Engelm.). The variability in tree species composition in the Blue Mountains leads to a variety of post-fire responses and exemplifies the importance of considering nuanced post-fire dynamics and their impacts on spectral trajectories.

Forests in the Blue Mountains, like throughout the western USA in general, have been indefinitely shaped by wildfire (Agee 1996). Many tree species have adapted to wildfire in different ways—various conifer species have thick bark, protecting meristematic tissue, phloem, and xylem (Pausas 2015) and, more specifically, lodgepole pines exhibit serotinous response, dispersing seeds en masse post-fire (Lotan 1976). Additionally, dominant shrubs, such as snowbrush ceanothus (*Ceanothus velutinus* Dougl. ex Hook.), have adapted to the fire regime by filling a niche as early post-fire colonizers, facilitated

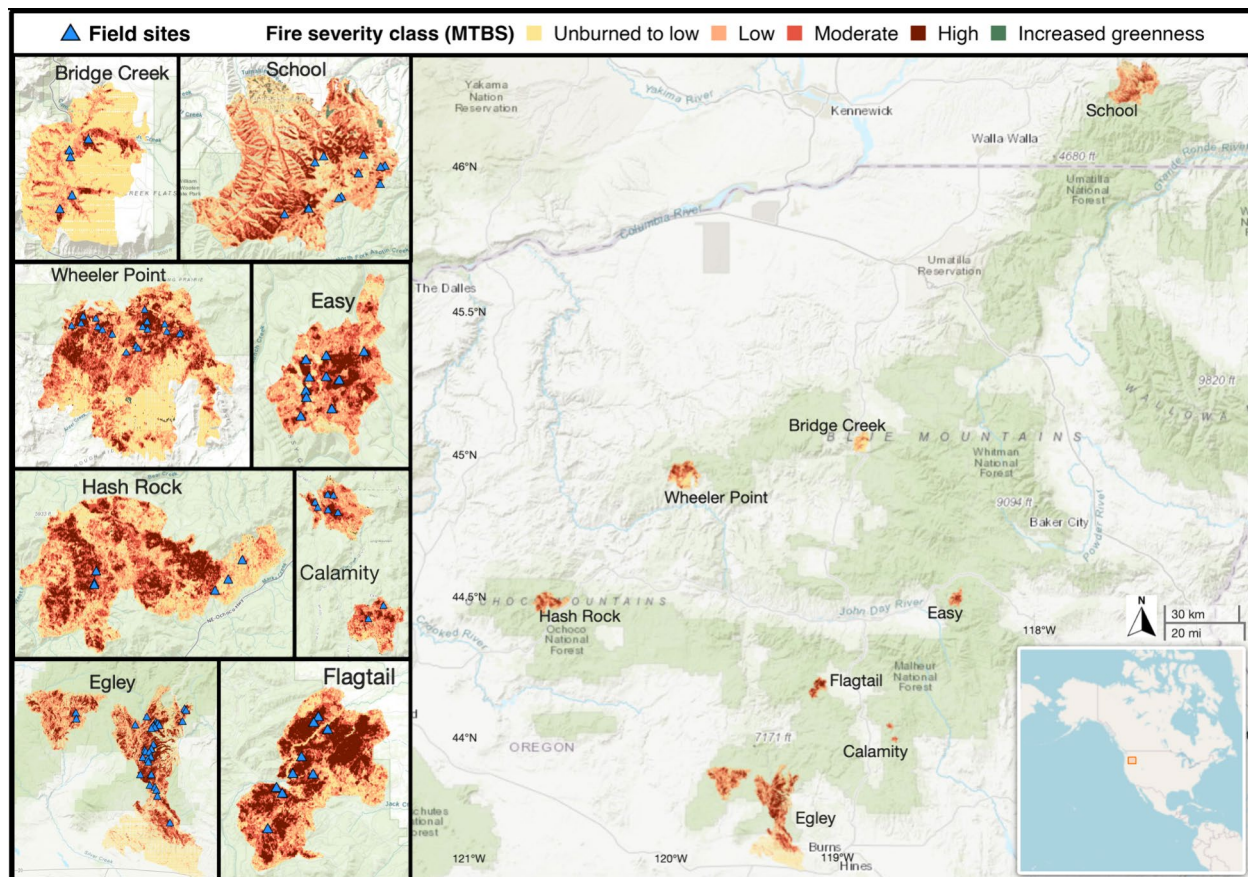


Fig. 1 A map of the study area and the eight sampled fires (see Table 1). Left panels display each fire, our field sites (blue triangles), and spatial distribution of the burn severity classes (as determined with monitoring trends in burn severity [MTBS] data) including unburned to low severity (light yellow), low severity (orange), moderate severity (red orange), high severity (dark red), and increased vegetation greenness (green). The right panel displays the locations and relative sizes of the sampled fires across the study area: the Blue Mountains, Oregon and Washington, USA

Table 1 Characteristics of the eight study fires in the Blue Mountains ecoregion: ignition dates (MTBS), field sampling year, number of field sites included in this study, size of fire (hectares), area impacted by high severity fire (hectares), proportion of high burn severity within the burn boundary, mean annual precipitation (mm; 30-year-normal for centroid of fire, PRISM), mean annual temperature (°C; 30-year-normal for centroid of fire, PRISM), and continuous heat-insolation load index (CHILI; mean value for random sample of points from high severity burn)

Fire	Ignition date	Sampling year	Field sites	Fire size (ha)	High severity fire (ha)	Proportion high burn severity	Mean annual precip. (mm)	Mean annual temp. (°C)	CHILI
Egley Complex	6 July 2007	2023	31	56,460	8440	0.149	413	5.7	176.7
School	5 August 2005	2021	12	20,923	2213	0.106	879	8.3	124.9
Wheeler Point	10 August 1996	2023	18	9174	1254	0.137	400	9.1	188.4
Hash Rock	23 August 2000	2022	6	6946	1201	0.173	560	7.1	173.2
Bridge Creek	13 August 2001	2022	5	3713	96	0.026	439	7.9	105.7
Flagtail	15 July 2002	2023	9	3234	1151	0.356	529	5.7	163.3
Easy	12 July 2002	2023	10	2590	463	0.179	815	5.6	159.8
Calamity Complex	6 July 2007	2023	8	943	123	0.130	484	6.1	181.4

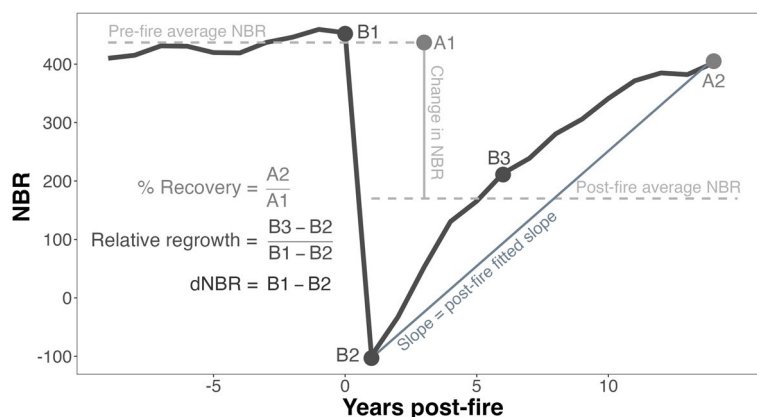


Fig. 2 The four spectral recovery metrics used in this study (change in NBR, % recovery, relative regrowth, and post-fire fitted slope), as displayed using a normalized burn ratio (NBR) time series for a pixel burned at high severity. Difference in NBR (dNBR) estimates burn severity and is used by monitoring trends in burn severity (MTBS) to determine burn severity classes

by fire-stimulated seeds, vigorous resprouting, and nitrogen-fixing capabilities (Binkley et al. 1982; Agee 1996; Anderson 2001). However, the natural fire regime that species have adapted to has been altered. Livestock grazing, timber harvest, and wildfire suppression limited the frequency of lower severity wildfire from approximately 1900 to 2000, and presently the Blue Mountains have denser and more homogeneous forests with increased fuel continuity leading to an increased frequency of large wildfires (>20,000 ha) since the 1980s (Hessburg et al. 2005, 2015). Due to unprecedented wildfire dynamics in the region, active land management to assist post-fire forest recovery is critical.

Site selection

To collect field measurements representing forest recovery, we sampled from 99 field sites in the Blue Mountains (Fig. 1, Table 1). We added 76 sites from five fires in 2023 to an existing network of 23 sites in high severity burned areas from 2021 (see Andrus et al. 2022) and 2022 (see Table 1 for plot count per fire and sampling years). Although sites burned at a low or moderate severity were sampled from in 2021 and 2022, we only considered sites burned at high severity (Monitoring Trends in Burn Severity [MTBS]; Eidenshink et al. 2007) in this study, to partially control for the effects of burn severity on post-fire recovery (Davis et al. 2023) and because land managers tend to prioritize high severity sites for active post-fire recovery projects. Site and fire selection differed slightly between 2023 and previous sample years. In 2023, we selected fires in (1) public forests (where forests were defined by $\geq 25\%$ pre-fire canopy cover with ≥ 5 m pre-fire vegetation height, using Landfire data; Rollins 2009); (2) areas with drier and hotter climates relative to the rest of the Blue Mountains (using 30-year-normals

for precipitation, temperature, and maximum vapor pressure deficit from parameter-elevation regressions on independent slopes model [PRISM Climate Group 2014] data); (3) locations not heavily sampled from in previous studies in the Blue Mountains (see Davis et al. 2023; exception: Egley Complex); (4) a gradient of climatic (using 30-year-normal PRISM climate data for mean annual precipitation and mean annual temperature) and topographic (using continuous heat-insolation load index, CHILI; Theobald et al. 2015) conditions; (5) a large enough high severity burn area to include at least eight sites spaced by >400 m (to limit spatial autocorrelation effects); and (6) the 1994 to 2008 timeframe to ensure that MTBS data and NBR data were readily available for at least 10 years pre-fire and 13 years post-fire (i.e., a sufficient period of detection for spectral recovery following Bright et al. 2019). In 2021 and 2022, we selected fires following considerations (1), (4), and (6).

In all cases, we sought to select sites across a gradient of climatic and topographic conditions from each fire whenever possible, we prioritized sites that were near (0.05 to 0.65 km) forest service roads, and we ensured that sites were at least 400 m apart to avoid spatial autocorrelation. In addition to the above considerations, to select sites for the fires selected in 2023, we conducted a *k*-means cluster analysis using four spectral recovery metrics (see Fig. 2, Table 2, and the “Remote sensing data” section) as input variables on a random sample of 1000 datapoints from sites classified as forest pre-fire which were impacted by high severity wildfire. *k*-means clustering is a commonly used data partitioning method, which groups data into a certain number (*k*) of clusters based on similarities between input variables (Steinley 2006). By using spectral recovery metrics as input variables in a *k*-means cluster analysis, the data are grouped

Table 2 Spectral recovery metrics used in this study, their formulas as presented utilizing normalized burn ratio (NBR) in their calculations (but spectral recovery metrics derived from normalized difference vegetation index [NDVI] were also considered [see Figs. S1–S2 and Tables S1–S2]), characteristics setting them apart from one another, and previous studies using a metric similar or identical to the described metric

Metric	Formula or calculation	Characteristics	References
Change in NBR	$NBR_{\text{mean 10years post-fire}} - NBR_{\text{mean 10years pre-fire}}$	Indicates average post-fire state relative to the average pre-fire state; partially determined by burn severity (dNBR)	Yang et al. (2017); see net change in evergreen NDVI (Kiel and Turner 2022)
% Recovery	$\frac{NBR_{\text{maximum post-fire}}}{NBR_{\text{mean pre-fire}}} \times 100\%$	Post-fire recovery in NBR relative to pre-fire mean NBR	Pickell et al. (2016); Bright et al. (2019)
Relative regrowth	$\frac{NBR_{\text{fitted, 5years post-fire}} - NBR_{\text{fitted, year of fire}}}{NBR_{\text{fitted, 1year post-fire}} - NBR_{\text{fitted, year of fire}}}$	Short-term (5 years) post-fire recovery relative to the burn severity (dNBR)	Kennedy et al. (2012); White et al. (2017)
Post-fire fitted slope	Slope of the fitted line from the minimum NBR value to 13 years post-fire	Spectral trajectory; how quickly the NBR increases 13 years post-fire	See NDVI trend (Fiore et al. 2020) and Thiel-Sen median slope estimate (Vanderhoof et al. 2021; Smith-Tripp et al. 2024)

into clusters with similar spectral trajectories. For the 1000-datapoint random sample, we selected a number of points from each fire proportional to the acres of high severity burn from that fire (see Table 1). We determined the optimal number of clusters ($k=3$) using a silhouette analysis and a total within sum of square analysis (R package factoExtra; Kassambara and Mundt 2020), where both analyses indicate within-cluster similarity and between-cluster dissimilarity. The k -means cluster analysis gave rise to data groupings, informed by spectral recovery metrics, which allowed for a stratified random sample of field sites representative of a variety of spectral recovery trajectories.

Field sampling

For every site from 2021 to 2023, we followed identical field sampling protocols. At each site, we measured vegetation cover and post-fire tree regeneration as field measurements of post-fire recovery in a circular plot (11.3 m radius, approximately 0.04 ha). From site center, we measured slope, aspect, elevation, and location (Trimble Geo7x, Trimble Inc., Westminster, CO; geo-positional root mean square accuracy: ± 5 cm) and recorded qualitative descriptions of the site. We also measured and identified trees to species, whenever possible, that died before or resulting from the fire to consider pre-fire state (i.e., conifer species composition).

For vegetation cover, we surveyed four 2×2 m fractional cover subplots 5 m from site center (downslope, upslope, and on the site contours). We determined percent cover estimates for functional groups—grasses, forbs, shrubs, and conifer seedlings and saplings. Conifer seedlings and saplings were grouped together, defined by diameter at “breast height” (DBH) of less than 10 cm, and their percent cover is referred to as % juvenile conifer

throughout the text. Fractional cover for each functional group was assessed independently to account for vertical heterogeneity. For example, if grasses grew underneath dense shrubs, we would measure the percent cover of those grasses as if the shrubs were not there, occasionally leading to the total percent cover of all groups adding up to over 100%. We also estimated canopy closure with a spherical densiometer facing downslope, upslope, and on the site contours at each fractional cover subplot.

For post-fire tree regeneration (including seedling and sapling establishment), we used a variable-width, 20-m-long transect along the site contour. Variable-width transects were necessary to account for differences in establishment density; in each case, we ensured that the measurements taken using the selected widths were representative of the site. In instances of dense seedling recruitment, such as sites exhibiting serotinous response of lodgepole pine (i.e., where there were typically more than 200 regenerating conifers in the site), we selected smaller transect widths (e.g., 2 to 5 m) to optimize time spent at the site. In instances where there was little to no recruitment (i.e., where there were typically less than 25 regenerating conifers in the site) regenerating, we selected larger widths (e.g., 10 to 20 m) to maximize representation of the site. Along with seedling and sapling counts, which we divided by site area to calculate seedling and sapling density, we identified species, and recorded heights, DBH (see above), status (e.g., alive, dying, dead), and indications of herbivory (e.g., no leading shoot, significant defoliation). For the full plot, we measured young trees (DBH > 10 cm, but post-fire establishment) and considered pre-fire state by measuring DBH, identifying species (when possible), and recording status (e.g., pre-fire mortality vs. wildfire-induced mortality, standing snag vs. stump vs. fallen, evidence of logging) for dead

or surviving trees. For a comprehensive measurement of post-fire regeneration density, we added the density of young trees to the seedling and sapling density.

Remote sensing data

We accessed multispectral data from the Landsat archive (USGS, NASA). Specifically, we gathered surface reflectance imagery data from Landsat Collection 2 at 30 m resolution, from 1984 to 2021 using LandTrendr implemented in Google Earth Engine (Gorelick et al. 2017; Kennedy et al. 2018). Additionally, we utilized LandTrendr, commonly used with temporally continuous remote sensing data to detect vegetation trajectories (Pérez-Cabello et al. 2021), to calculate spectral indices used in this analysis from Landsat data. Multispectral Landsat images were identified for the study area and filtered to include only those collected during the growing season (1 June to 31 August) each year (1984 to 2021). Pixels obscured by snow, clouds, or cloud shadows were masked out. We used selected images to generate rasters of annual growing season values for each spectral band using the medoid selection process described by Kennedy et al. (2018). These annual composite rasters were then used to calculate annual NBR values using near infrared (NIR) and short-wave infrared (SWIR) wavelengths (Eq. 1), and raster stacks of annual NBR values were exported for each study fire. NBR was extracted from raster stacks and time series data frames were formulated and used for further analyses. For each fire, we utilized 10 years of pre-fire and 13 years of post-fire NBR data (following Bright et al. 2019). We calculated four spectral trajectory metrics from the NBR time series (Fig. 2; Table 2) to represent different components of spectral recovery in our site selection and analyses. Although we primarily considered NBR-derived spectral recovery metrics (Fig. 2; Table 2), we also performed identical data processing and calculations for the normalized difference vegetation index (NDVI; Eq. 2), which is used in many studies investigating spectral recovery (e.g., Yang et al. 2017; Fiore et al. 2020; Vanderhoof et al. 2021; Kiel and Turner 2022).

$$NBR = \frac{NIR - SWIR}{NIR + SWIR} \quad (1)$$

$$NDVI = \frac{NIR - Red}{NIR + Red} \quad (2)$$

Datasets and variables

In statistical analyses, we used spectral recovery metrics (Fig. 2, Table 2) and burn severity (dNBR; Fig. 2) along with field measurements: fractional cover estimates (%

shrub, % grass, % forb, % juvenile conifer), canopy closure, regeneration density, slope, and aspect (cosine-transformed). Although this study focused on sites burned at a high severity, including dNBR in analyses allowed us to consider variation in burn severity within the high burn severity class defined by MTBS. We also used elevation and location (Trimble Geo7x) in analyses along with the topographic metric, continuous heat-insolation load index (CHILI; Theobald et al. 2015). In addition to remote sensing and field data, we incorporated external datasets: PRISM, Climate North America (Climate NA; Wang et al. 2016), Landfire (Rollins 2009), and US Forest Service International Tree Species Parameter Mapping (ITSPM; Ellenwood et al. 2015). Using PRISM yearly climate data (see Fig. S3; PRISM Climate Group 2014), we calculated post-fire averages (1 to 5 years post-fire) for precipitation, mean temperature, and maximum vapor pressure deficit, and we also gathered PRISM 30-year-normal values for the above climatic metrics. We gathered cumulative water deficit data (CWD) from Climate NA for analyses and to define the trailing edge (TE). Landfire data provided information about pre-fire canopy cover, which we used in analyses and to define the extent of forests. Lastly, ITSPM data informed pre-fire species composition, as we gathered data on the ranges of ponderosa pine, lodgepole pine, Douglas-fir, grand fir, western larch, and Engelmann spruce. We cross-validated ITSPM data with our field-based species identification of trees that died resulting the fire or pre-fire.

Statistical analyses

Spectral recovery vs. field measurements: top-down approach

We compared spectral recovery to field measurements of post-fire vegetation dynamics with a top-down approach (i.e., from the spectral trajectory perspective). To determine differences in spectral recovery, we performed a *k*-means cluster analysis (Steinley 2006) using spectral recovery metrics (Table 2) as input variables. To supplement the spectral recovery metrics derived from 99 field sites, we randomly sampled 586 additional points from high severity burn areas from the sampled fires. For each fire, the number of points in the random sample was proportional to the acres of high severity burn (see Table S3) and we buffered points so that they were at least 400 m apart from each other. We determined the optimal number of clusters (*k*=2) using silhouette and total within sum of square analyses (R package factoextra; Kassambara and Mundt 2020). With two clusters and the spectral recovery metrics as input variables, the *k*-means clusters represented two modes of spectral recovery. First, we contrasted the modes of spectral recovery using time series of baseline-adjusted NBR. We calculated

baseline-adjusted NBR as the difference between NBR and a baseline pre-fire mean NBR value (1 to 10 years pre-fire) for each location, allowing us to isolate post-fire differences in NBR trajectories. We also considered the relativized difference in normalized burn ratio (RdNBR), commonly utilized by land managers as a measurement of burn severity adjusted for the pre-fire state (Fig. S4); however, we primarily utilized baseline-adjusted NBR or baseline-adjusted NDVI in time series visualizations due to their closer resemblance to NBR and NDVI time series presented in other spectral recovery studies (Kennedy et al. 2012; White et al. 2017; Bright et al. 2019). By running analyses of variance adjusted for the random effect of fire (RANOVAs), we determined whether the two spectral recovery modes diverged and the timing of divergence. Next, to compare spectral recovery to field measurements, we compared k -means clusters to field, topographic, climate, and multispectral data. Using RANOVAs, we tested whether the k -means cluster had a significant ($\alpha=0.05$) effect on field measurements (% shrub, % grass, % forb, % juvenile conifer, regeneration density, and canopy closure), topographic variables (elevation and slope), and the four spectral recovery metrics (see Table 2).

Spectral recovery vs. field measurements: bottom-up approach

We compared post-fire vegetation dynamics to spectral recovery with a bottom-up approach (i.e., from the field observations perspective). We performed a k -means cluster analysis using the field measurements as input variables and $k=3$ clusters representing modes of post-fire vegetation composition. Mirroring the top-down approach, we visualized the effect of field data on spectral recovery with a baseline-adjusted NBR time series. With RANOVAs and post hoc Tukey–Kramer tests (adjusted for random effects, R package emmeans; Lenth 2021), we determined significant differences ($\alpha=0.01$) between k -means clusters in the baseline-adjusted NBR time series, allowing us to ensure that the three k -means clusters showcased significant differences in field metrics (% grass, % shrub, % juvenile conifer, and regeneration density), and determined if there were significant differences in spectral recovery metrics between the three k -means clusters.

Predicting field measurements of forest recovery using climatic, topographic, and multispectral data

To investigate how post-fire climate, topography, and spectral recovery relate to field measurements of post-fire vegetation dynamics, we conducted generalized linear mixed effects model selections (R package glmTMB; Brooks et al. 2017) to predict % grass, % shrub, %

juvenile conifer, and regeneration density. Because of the hierarchical data structure, with multiple sites sampled from each fire scar, we accounted for the random effect of fire. Models with multicollinearity, as determined when the variance inflation factor (VIF) was greater than 4 (Daoud 2017; Kim 2019), were eliminated from selection. We selected predictors and interaction terms primarily using Akaike's information criterion (AIC; Akaike 1974) and secondarily using Bayes' information criterion (BIC; Neath and Cavanaugh 2012) by minimizing AIC and BIC values. In cases where both Δ AIC and Δ BIC were less than two (i.e., models were not significantly different for either criterion), we determined top-performing models by investigating Kenward-Roger approximated p -values (Luke 2017) for each predictor and Nakagawa's marginal and conditional R^2 (Nakagawa and Schielzeth 2013). The response variable informed which model families we considered: for % cover metrics, Gaussian or Binomial model families were considered, while for regeneration density, Gaussian, Poisson, and Negative Binomial Types I and II were considered (Zuur et al. 2009). To determine exactly which model family to use for each response variable, we compared diagnostic plots (e.g., QQ-plots, residuals vs. predicted plots; R package DHARMA; Hartig 2022) for each considered model family. Furthermore, we tested if accounting for zero inflation was necessary using R package DHARMA (function "testZeroInflation"; Hartig 2022) and by comparing AIC values of models with and without accounting for zero inflation. Models accounting for zero inflation by predicting presence and absence utilized a variable selection process mirroring the selection of predictors in the main model—primarily considering AIC and using BIC, Kenward-Roger approximated p -values, and Nakagawa's marginal and conditional R^2 if needed.

To differentiate relative predictive capabilities of spectral, climatic, and topographic metrics on field measurements of post-fire forest recovery and community composition, we completed the above model selection process three times. The first set of models included only post-fire climate metrics and topographic metrics. The second set of models included only spectral recovery metrics (Table 2), dNBR, and pre-fire canopy cover (Landfire). Lastly, we considered all predictors to investigate whether using multispectral data in-tandem with climate and topography data could improve predictions of where post-fire forest recovery occurs.

Juxtaposing relationships in the trailing edge and non-trailing edge sites

Based on field observations and previous studies (Parks et al. 2019), we expected different post-fire recovery outcomes in trailing edge (TE) and non-trailing edge (non-TE) sites; therefore, we investigated how relationships

between climate, spectral recovery, and field measurements of post-fire vegetation dynamics differed in TE versus non-TE sites. We defined the TE using present (1981 to 2010) CWD (Climate NA) and future (2041 to 2070; average of RCP 8.5 projections) CWD in the forested areas of the Blue Mountains ecoregion (as in Meigs et al. 2023), where we utilized the 95th percentile of present CWD as the TE threshold. We defined locations with future projections of CWD higher than this threshold as TE, while we defined other locations as non-TE. We formulated generalized linear mixed effects models to differentiate contributions of remote sensing and climate data on field measurements in the TE and non-TE sites. Informed by the first model selections, post-fire fitted slope represented spectral recovery, while post-fire precipitation represented climate. Moreover, the same model families as selected in the first model selection were utilized in these models. Each model accounted for zero inflation using an intercept-only model. We included a TE factor in interaction terms with post-fire fitted slope and post-fire precipitation in these models. Using RANOVAs, we investigated how field metrics and post-fire fitted slope differed between TE and non-TE sites. Lastly, we investigated differences in pre-fire species composition (field-validated ITPSM data) between the TE and non-TE sites.

Results

Spectral recovery versus field measurements: top-down approach

The top-down *k*-means cluster analysis resulted in “fast recovery” and “slow recovery” clusters, informed by spectral recovery metrics, that diverged 4 years post-fire ($P \leq 0.001$; Fig. 3a). For the fast recovery cluster, all four spectral recovery metrics (input variables) were higher than in the slow recovery cluster ($P \leq 0.001$; Fig. 3b–e). Field measurements differed between spectral recovery clusters. A fast spectral recovery was associated with higher % shrub cover ($P \leq 0.001$; Fig. 3h) and a lower % grass cover ($P = 0.021$; Fig. 3i) relative to the slow recovery cluster. We found no significant differences between spectral recovery clusters for % juvenile conifer ($P = 0.16$; Fig. 3f) or regeneration density ($P = 0.19$; Fig. 3g). Otherwise, the fast recovery cluster was typically impacted by lower severity wildfire (dNBR; $P = 0.005$) than the slow recovery cluster (Fig. S5). The top-down *k*-means cluster analysis with NDVI-derived spectral recovery metrics yielded similar results to the NBR-based analysis. However, in the NDVI-based analysis, fast recovery and slow recovery clusters diverged 2 years earlier than in the NBR-based analysis, with baseline-adjusted NDVI values significantly differing after 2 years post-fire ($P \leq 0.001$; Fig. S1).

Spectral recovery versus field measurements: bottom-up approach

The bottom-up *k*-means cluster analysis resulted in “grass-dominated”, “shrub-dominated”, and “tree-dominated” clusters (Fig. 4). These *k*-means clusters had different spectral trajectories, as grass-dominated sites had the slowest spectral recovery while shrub-dominated and tree-dominated sites had similar spectral recoveries (Fig. 4a). Examining the NBR time series, the spectral signatures of grass-dominated and shrub-dominated sites diverged 5 years post-fire and the shrub-dominated sites had higher baseline-adjusted NBR values every year after that ($P \leq 0.001$). The spectral signatures of grass-dominated and tree-dominated sites did not diverge until 13 years post-fire ($P \leq 0.001$; Fig. 4a). Importantly, there were differences in the spectral recovery metrics between bottom-up *k*-means clusters; RANOVA and Tukey–Kramer tests indicated that the shrub-dominated cluster had a faster spectral recovery than the grass-dominated cluster reflected by all four spectral recovery metrics ($P \leq 0.001$ for post-fire fitted slope, % recovery, and relative regrowth, Fig. 4c–e; and $P = 0.002$ for change in NBR, Fig. 4b). The tree-dominated cluster only significantly differed from either of the other clusters when assessing % recovery, in which the tree-dominated cluster had a higher % recovery than the grass-dominated cluster ($P = 0.021$, Fig. 4c). Otherwise, the grass-dominated cluster had higher % grass than the other *k*-means clusters ($P \leq 0.001$), the shrub-dominated cluster had higher % shrub than the other *k*-means clusters ($P \leq 0.001$), and the tree-dominated cluster had higher % juvenile conifer ($P \leq 0.001$) and log-transformed regeneration density ($P \leq 0.001$) than the other *k*-means clusters (Fig. 4f–i). A bottom-up *k*-means cluster analysis using NDVI-derived metrics yielded slightly different results, as the tree-dominated cluster and grass-dominated cluster differed significantly when assessing % recovery, change in NDVI, and post-fire fitted slope (Fig. S2b–d). Moreover, in the NDVI-based analysis, the spectral signatures of grass-dominated and tree-dominated sites diverged 11 years post-fire ($P \leq 0.001$; Fig. S2a), 2 years earlier than in the NBR-based analysis.

Predicting field measurements of forest recovery using climatic, topographic, and multispectral data

Three generalized linear mixed effects model selections using (1) spectral recovery metrics, (2) climate and topography metrics, and (3) all predictors exhibited potential benefits of involving multispectral data along with climate data when predicting post-fire forest recovery (Table 3). For regeneration density, % juvenile conifer, and % grass, top-performing models included a combination of spectral recovery and climate metrics.

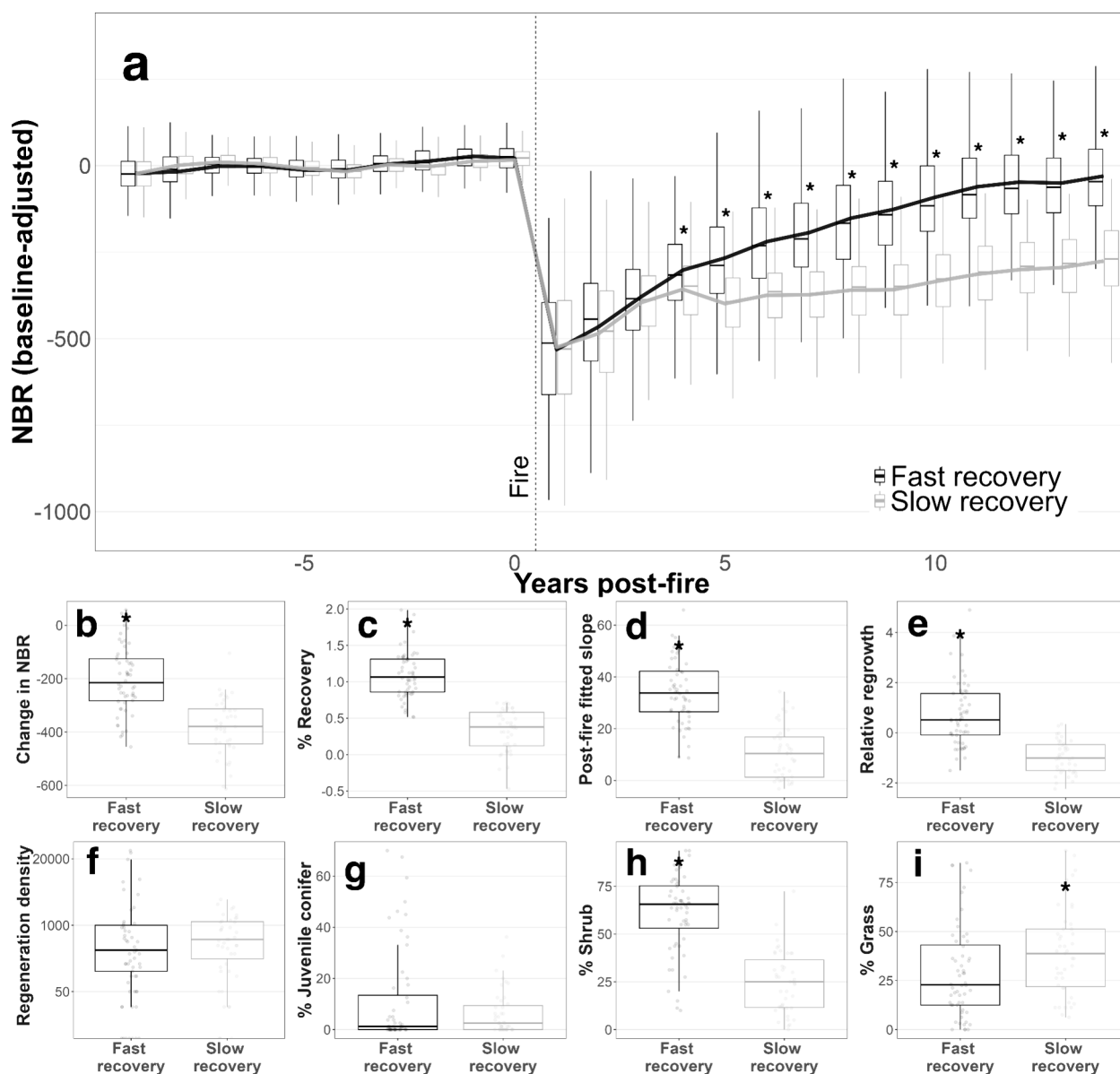


Fig. 3 Baseline-adjusted normalized burn ratio (NBR) over time for “fast recovery” (dark gray; $n=58$) and “slow recovery” (light gray; $n=41$) k -means clusters with asterisks indicating years which the two clusters had significant ($P < 0.01$) differences in the baseline-adjusted NBR (a). Boxplots of the spectral recovery metrics (k -means cluster analysis input variables; b–e) and selected field measurements (f–i) with asterisks indicating cases when one cluster had a significantly ($P < 0.05$) higher value than the cluster without an asterisk displayed. In the boxplots, the thick horizontal line within the box represents the data median, while the lower and upper limits of the box represent the interquartile range (IQR; 25th to 75th percentiles), and vertical lines extending above and below the boxes (the “whiskers”) represent 1.5 times the IQR or the minimum and maximum values

For % shrub, the top-performing model solely included spectral recovery metrics. Topographic metrics were not included in any top-performing models. Post-fire fitted slope proved to be a key spectral recovery metric, as it was included in top-performing models predicting % juvenile conifer, % shrub, and % grass. Otherwise, post-fire precipitation proved to be a key climatic predictor,

as it was included in top-performing models predicting regeneration density, % juvenile conifer, and % grass. Similar results were observed when using NDVI-derived spectral recovery metrics, as the top-performing models for regeneration density, % juvenile conifer, and % grass included spectral recovery, climate, and topography predictors (Table S1).

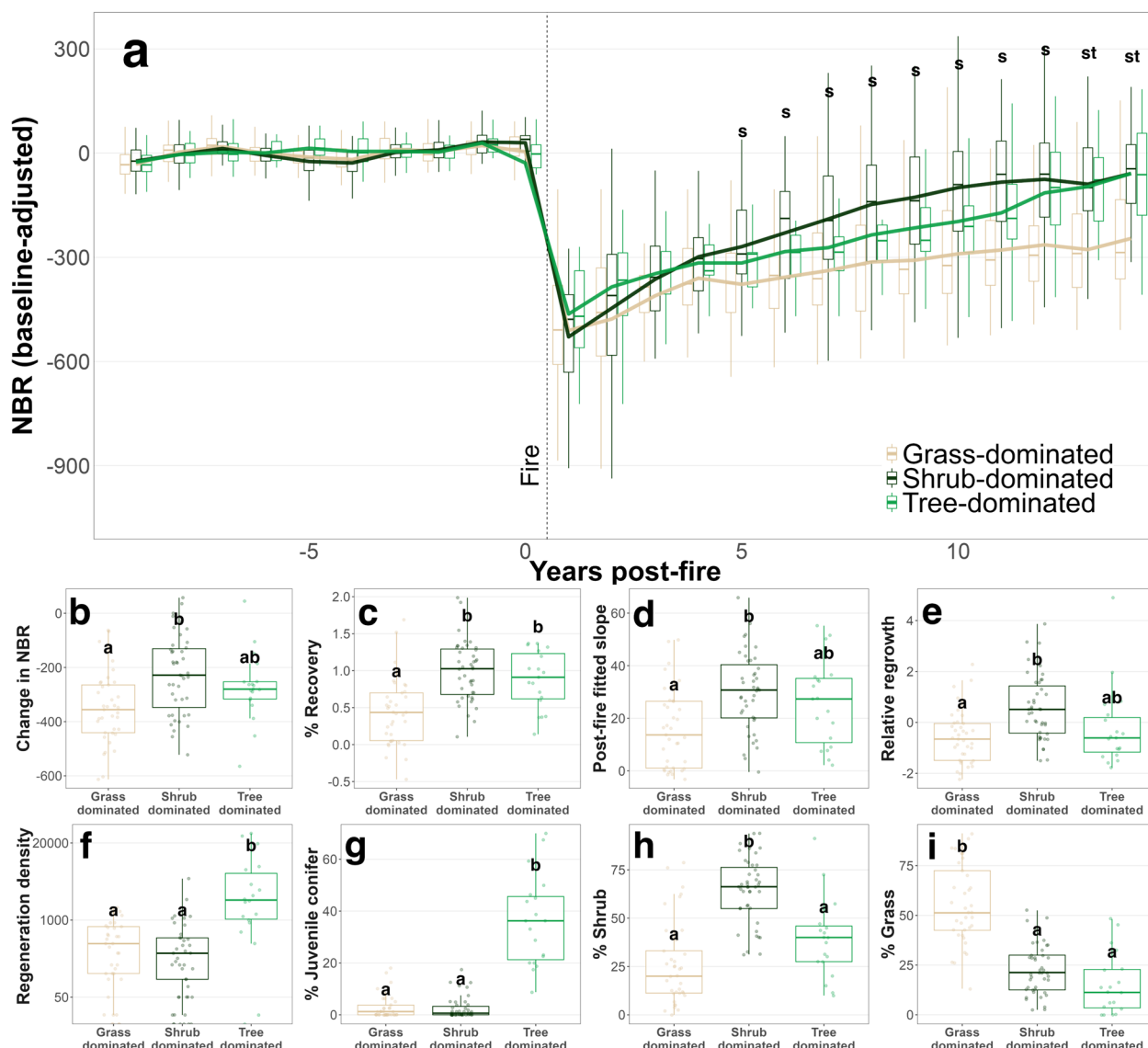


Fig. 4 Baseline-adjusted normalized burn ratio (NBR) over time for three *k*-means clusters representing grass-dominated (tan; $n = 37$), shrub-dominated (dark green; $n = 43$), and tree-dominated (light green; $n = 19$) sites (a). Significant divergence ($P < 0.01$) between clusters is shown with letters where: “s” indicates significant differences between shrub-dominated and grass-dominated clusters and “st” indicates significant differences between tree-dominated and grass-dominated clusters and between shrub-dominated and grass-dominated clusters (a). Boxplots of spectral recovery metrics (b–e) and field metrics (*k*-means cluster analysis input variables; f–i) with Tukey-Kramer results indicated with letters where, if the same letter is displayed over the *k*-means cluster, there is no significant ($P > 0.05$) differences between those clusters for the presented variable (i.e., “ab” is similar to both “a” and “b”)

Comparing relationships in the trailing edge and non-trailing edge sites

The trailing edge (TE) sites ($n = 59$) and non-trailing edge (non-TE) sites ($n = 40$) had different relationships between post-fire forest recovery and spectral recovery (Fig. 5). The interaction terms between post-fire fitted slope and the TE were significant for regeneration density ($P = 0.035$) and % juvenile conifer ($P = 0.006$) and had negative coefficients for both cases (Fig. 5a).

Coefficients for interaction terms between post-fire precipitation and the TE were positive for regeneration density, % juvenile conifer, % shrub, and % grass (Fig. 5a). Although we observed greater rates of conifer regeneration at non-TE sites and the trends in the data supported these observations, there was not significantly higher % juvenile conifer ($P = 0.13$) or regeneration density ($P = 0.20$) at the non-TE sites relative to the TE sites (Fig. 5b). However, there was higher % shrub

Table 3 Three generalized linear mixed effects model selections using: (1) climate and topography metrics, (2) spectral recovery metrics, and (3) all predictors. The third model selection (3) included all predictors shown in selections (1) and (2); however, predictors indicated with an asterisk in (1) or (2) were not selected for in (3); therefore, they were omitted from that portion of the table. Bolded text indicates the top-performing models out of all three model selections. Coefficients for variables selected in the top-performing model are displayed along with their significance (Kenward-Roger *p*-value; *0.05 > *P* > 0.01, **0.01 ≥ *P* > 0.001, ****P* ≤ 0.001), while empty cells indicate that the predictor was not selected for in the model selection. Model family, zero inflation terms (if applicable), interaction terms, AIC, BIC, and Nakagawa’s marginal and conditional *R*² are all displayed. For interaction terms and zero inflation terms, the following terms were abbreviated as shown: continuous heat-insolation load index (CHILI), post-fire precipitation (Precip.), post-fire temperature (Temp.), elevation (Elev.), relative regrowth (R.R.), post-fire fitted slope (PFFS), and pre-fire canopy cover (C.C.)

	Model family:	Regeneration density	% Juvenile conifer	% Shrub	% Grass
		Neg. binomial (II)	Gaussian	Gaussian	Gaussian
(1) Climate and topography	Elevation	-	-	8.96**	-
	Slope	-	-	9.40**	-
	CHILI*	-0.239	-	-	-
	Transformed aspect	-0.039	-	3.98	-3.86
	Post-fire precipitation	0.974***	9.64***	-	-10.84***
	Post-fire temperature	-	-3.74	-	-
	Post-fire maximum VPD*	-	-	-	-
	Interaction terms	CHILI:Aspect -0.956***	Precip.:Temp. -7.76**	Elev.:Slope 2.04	None
	Zero inflation term(s)	Intercept -2.06***	Elev. + Precip. -0.264 & -0.866**	None	Precip. 4.88
	AIC / BIC	1362.8 / 1383.2	580.0 / 602.9	877.1 / 894.9	841.4 / 859.2
(2) Spectral recovery	Marginal / conditional <i>R</i>²	0.37 / 0.53	0.83 / 0.87	0.14 / NA	0.72 / 0.87
	Change in NBR	-	10.87**	15.47***	-
	Post-fire fitted slope	-	7.77***	9.71***	-1.76
	% Recovery*	-	-	-	-
	Relative regrowth	-0.410**	-11.92***	-	0.501
	Burn severity (dNBR)	-	-	6.51**	-
	Pre-fire canopy cover*	0.722***	6.91**	-	-1.66
	Interaction terms	R.R.:C.C. -0.430**	None	None	PFFS:R.R. 3.61***
	Zero inflation term(s)	Intercept -2.08***	C.C. -0.785**	None	PFFS 1.16
	AIC / BIC	1371.3 / 1389.1	580.0 / 602.8	805.2 / 820.5	845.0 / 867.9
Marginal / conditional <i>R</i>²	0.21 / 0.55	0.81 / 0.88	0.59 / NA	0.49 / 0.90	
(3) All predictors	Elevation	-	-	-	-
	Slope	-	-	-	-
	Transformed aspect	-	-	-	-
	Post-fire precipitation	0.769**	6.41**	-	-10.55**
	Post-fire temperature	-0.087	-	-	-5.35
	Change in NBR	-	-	15.47***	-
	Post-fire fitted slope	-	4.77*	9.71***	-6.85**
	Relative regrowth	-0.531***	-4.74*	-	-
	Burn severity (dNBR)	-	-	6.51**	-
	Interaction terms	R.R.:Temp. 0.625***	PFFS:Precip. 5.913***	None	PFFS:Temp. -9.612***
	Zero inflation term(s)	Intercept -2.06***	C.C. -0.793***	None	PFFS 1.13
	AIC / BIC	1358.0 / 1378.3	564.0 / 586.9	805.2 / 820.5	834.9 / 857.8
	Marginal / conditional <i>R</i>²	0.34 / 0.49	0.77 / 0.92	0.59 / NA	0.76 / 0.94

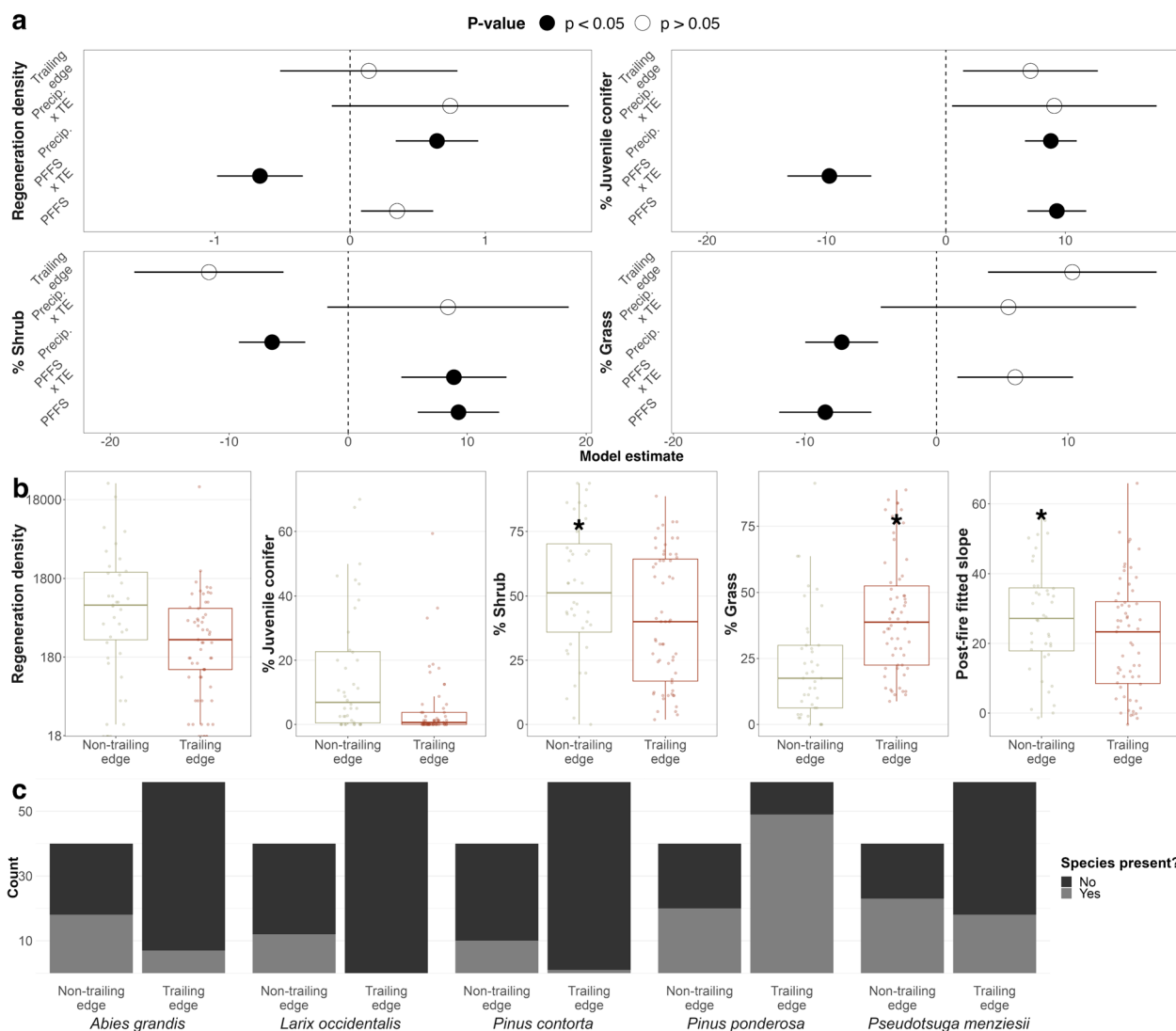


Fig. 5 Model estimates and standard errors from generalized linear mixed effects models predicting regeneration density, % juvenile conifer, and % shrub using post-fire fitted slope (PFFS), post-fire precipitation (Precip.), a trailing edge factor (TE), and interactions between TE and post-fire fitted slope where significant predictors ($P < 0.05$) are indicated with closed points (a). Boxplots showing differences in field measurements and post-fire fitted slope between TE and non-TE sites with significance (RANOVA, $P < 0.05$) indicated with asterisks (b). The presence of selected conifer species in TE and non-TE sites (c)

($P \leq 0.001$) in non-TE sites and significantly higher % grass ($P = 0.045$) in TE sites (Fig. 5b). Moreover, spectral trajectories of non-TE sites were quicker ($P = 0.009$) than in TE sites (as shown with post-fire fitted slope in Fig. 5b; also see Fig. S6). Through cross-validated ITPSM data, we observed key differences in the conifer species present across the TE and non-TE sites, as western larch (*Larix occidentalis*) and lodgepole pine (*Pinus contorta*) were almost solely present in non-TE sites, while TE sites were largely composed of ponderosa pine (*Pinus ponderosa*) and Douglas-fir (*Pseudotsuga menziesii*) (Fig. 5c).

Discussion

Previous studies have utilized spectral recovery to represent post-fire recovery (Kennedy et al. 2012; White et al. 2017; Bright et al. 2019; Chuvieco et al. 2020); however, it remains unclear under what circumstances spectral recovery represents forest recovery versus the recovery of other vegetation types. We investigated relationships between spectral trajectories and field measurements of post-fire vegetation dynamics with top-down (Fig. 3) and bottom-up (Fig. 4) approaches. We found that the vegetation dynamics detected by spectral recovery differed with ecological context. A fast spectral recovery

more often corresponded with regenerating shrubs than conifer recovery throughout the study area, but in non-trailing edge sites specifically, a fast spectral recovery aligned with conifer recovery and regenerating shrubs. Although the relationship between spectral and forest recovery varied with ecological setting, the inclusion of spectral recovery metrics in generalized linear mixed effects models consistently improved predictions of conifer recovery (% juvenile conifer and regeneration density; Table 3, Table S1). This suggests that the performance of models predicting post-fire forest recovery, which currently rely primarily on climatic and topographic data (e.g., Davis et al. 2023), could be improved by incorporating multispectral data. Our study in the Blue Mountains showcases the importance of the field validation of spectral recovery, identifies potential pitfalls of using spectral recovery as a proxy for forest recovery, and provides insights regarding how multispectral data can be useful when investigating post-fire recovery dynamics.

Patterns of spectral recovery can be attributed to varying vegetation dynamics

The top-down *k*-means cluster analysis revealed that field sites with a fast spectral recovery were often dominated by shrubs (Fig. 3h), with no distinct differences in conifer recovery (% juvenile conifer and regeneration density) between fast and slow recovery clusters (Fig. 3f, g). Likewise, the bottom-up *k*-means cluster analysis revealed that shrub-dominated field sites had a faster spectral recovery, especially compared to grass-dominated sites (Fig. 4a). We largely attributed the fast spectral recovery of regenerating shrubs to the evergreen shrub, snowbrush ceanothus (*Ceanothus velutinus*). A common shrub in early successional communities, snowbrush ceanothus vigorously resprouts post-fire and forms dense homogeneous stands in high severity burn areas throughout the study area (Anderson 2001). Furthermore, the nitrogen-fixing properties of snowbrush ceanothus may facilitate seedling establishment over the course of decades, suggesting that shrub-dominated sites may eventually yield to forest recovery (Binkley et al. 1982; Agee 1996). Spectral recovery metrics could be calculated with longer time series of multispectral data to differentiate between cases where shrubs, like snowbrush ceanothus, facilitate forest recovery and cases where shrubs persist on the landscape and inhibit forest recovery through competition. Similarly, collecting field data at longer intervals (> 25 years post-fire) or resurveying field sites could track shrub- or grass-dominated sites to determine whether succession leads to forest recovery or vegetation type conversion. Regardless, the limited conifer recovery in shrub- and grass-dominated sites (see

Fig. 4f, g) may indicate decreasing forest resilience in the face of climate change and increasing wildfire frequency and severity (Parks et al. 2018; Coop et al. 2020; Parks and Abatzoglou 2020; Hagmann et al. 2021).

Post-fire recovery outcomes vary widely in mixed conifer forests, presenting a considerable challenge: how can we determine when and where it is appropriate to use spectral recovery trajectories to detect forest recovery versus vegetation transitions? In our study, tree-dominated and shrub-dominated sites showed similar spectral trajectories 1 to 12 years post-fire (Fig. 4a) despite vast ecological, economical, and cultural differences between the two vegetation types (Stine et al. 2014). Researchers have previously attempted to differentiate between conifer recovery and shrub regeneration by using multispectral data from fall, winter, and spring months to isolate conifer trees from deciduous shrubs and trees (Vanderhoof et al. 2021; Kiel and Turner 2022), but these protocols are not expected to distinguish between conifers and evergreen shrubs when assessing spectral recovery over short time periods (i.e., before the height of conifers exceeds the maximum expected height of evergreen shrubs). Compared to shrub- and tree-dominated sites, grass-dominated sites exhibited a particularly slow spectral recovery (Fig. 4). Grass- and shrub-dominated sites had distinct spectral signatures as soon as 4 years post-fire (Fig. 4a; also see Fig. 3i and Fig. S2a), while the spectral trajectories of grass- and tree-dominated sites diverged as soon as 11 years post-fire (Fig. S2a; or 13 years post-fire; Fig. 4a). In this case, the clear divergence of grass-dominated spectral trajectories suggests that transitions to grasslands or successional patterns, depending on regional vegetation dynamics and characteristics, can potentially be detected with multispectral data.

Spectral recovery studies often analyze post-fire recovery over brief periods unrepresentative of the expected duration of recovery of mixed conifer forests following a high severity fire. For example, Meng et al. (2015) include data up to 5 years post-fire and Bright et al. (2019) include data 13 to 20 years post-fire; however, the mixed conifer and ponderosa pine forests in those studies are expected to take longer than 20 years to recover from a high severity burn (Stevens-Rumann et al. 2022; Agee 1996). Similarly, in our study spectral recovery metrics gathered over a 13-year-period were insufficient to parse recovering vegetation into recovering forest versus regenerating shrubs without additional data inputs. To confront this challenge, future studies could identify spectral signatures which align with different post-fire recovery outcomes and could utilize climate, topography, and pre-fire community composition in-tandem with multispectral data to predict post-fire vegetation dynamics.

Multispectral data can improve predictions of post-fire forest recovery

Top-performing models predicting field measurements of forest recovery included both spectral recovery metrics and post-fire climate metrics as predictors (model selection 3, Table 3, Table S1). Consequently, we demonstrate (building upon previous mapping of post-fire recovery probability using climate and topography; Davis et al. 2023; see Fig. S7) that supplementing models with multispectral data could improve predictions of forest recovery. Post-fire precipitation was consistently selected for in top-performing models for regeneration density, % juvenile conifer, and % grass signifying the vital role that precipitation plays in the dichotomy of forest recovery versus transition to grasslands. Climate and topography (model selection 1) explained differences in post-fire forest recovery better than multispectral data alone (model selection 2; Table 3). Specifically, post-fire precipitation, transformed aspect, and CHILI performed well in predicting regeneration density, indicating that higher densities of recovering conifers were observed in wetter sites (as in Andrus et al. 2022; Davis et al. 2023) with less solar exposure (as in Boag et al. 2020). Conifer recovery exhibited stronger relationships with post-fire precipitation than any given spectral recovery metric (Fig. S8) further aligning with expected limitations of water availability on post-fire recovery. Despite more apparent links between conifer recovery and post-fire climate, the inclusion of spectral recovery metrics improved the performance of models predicting conifer recovery (Table 3).

To further investigate potential benefits of introducing spectral recovery metrics into predictive models for forest recovery, future work could formulate spatial models akin to Davis et al. (2023) using multispectral data in tandem with climatic and topographic data. However, until multispectral data are adequately implemented in spatial predictive models, field-validated models utilizing climatic and topographic data (e.g., Davis et al. 2023) can inform decision making about post-fire land management. Moreover, models predicting post-fire recovery could inform climate-adaptive decision making (see Davis et al. 2024). For example, the Resist-Accept-Direct (RAD) framework (Schuurman et al. 2020, 2022) outlines three decision pathways: (R) resisting vegetation conversion through active land management (e.g., planting), (A) accepting vegetation conversion and conserving resources when reforestation efforts are likely to fail, and (D) directing vegetation conversion to a climate-wise alternative state. Robust models predicting post-fire vegetation dynamics could identify likelihood of natural forest recovery or vegetation conversion, thus guiding which RAD decision pathway(s) to consider. By accounting for climate adaptation in active management, land

management organizations' limited time and resources can be better-allocated, as they ramp up reforestation efforts in response to recent policy developments (e.g., REPLANT Act of 2021).

Spectral recovery has different ecological meaning in different contexts

By investigating trailing edge (TE) and non-trailing edge (non-TE) forests, we uncovered different relationships between spectral recovery and forest recovery (Fig. 5). When predicting conifer recovery (regeneration density and % juvenile conifer), positive coefficients for post-fire fitted slope suggested that conifer recovery aligned with faster spectral recovery in non-TE forests, while negative interactions between TE and post-fire fitted slope indicated that this was not the case in TE forests (Fig. 5a). Fast-growing conifer species such as lodgepole pine and western larch were more common in non-TE forests (Fig. 5c), where links between spectral and forest recovery were more evident (Fig. 5a) and spectral recovery was significantly faster (Fig. 5b). Unlike slower-growing conifers, such as ponderosa pine and Douglas-fir, lodgepole pine and western larch establish abundantly post-fire (e.g., lodgepole pines' serotinous response) and grow rapidly (Agee 1996). Additionally, non-TE forests boast favorable conditions for post-fire forest recovery (i.e., they are cooler and wetter than TE forests; Fig. S6); thus, they are more likely to support young conifers than TE forests. The contrast between TE and non-TE forests demonstrates the importance of considering different ecological contexts when assessing the potential of spectral recovery to indicate forest recovery.

Mixed conifer forests showcase considerable variability in community composition pre-fire and post-fire, as grasses, shrubs, and conifer trees can all inhabit the landscape in different assemblages which fluctuate over time (Agee 1996). Based on our definition of trailing edge and our understanding of the study area, TE forests are more likely dry mixed conifer forests while non-TE forests are more likely moist mixed conifer forests (see Fig. 5c). The management of these units differs. Correspondingly, models predicting forest recovery should account for the variable vegetation and ecology of dry and moist mixed conifer forests by including information describing the pre-fire community. In ecological contexts with less variability in post-fire vegetation dynamics (e.g., chaparral; see Storey et al. 2016), we posit that multispectral data may better align with post-fire recovery. In chaparral, post-fire dynamics are predominantly characterized by resprouting and reseeding shrubs (Keeley and Keeley 1981; Park and Jenerette 2019); therefore, the recovering vegetation reflected by spectral recovery is most likely chaparral. Similarly, in relatively dense forests impacted

by low-to-moderate severity wildfires, amplified roles of existing seed sources facilitating forest recovery and the spectral signal of surviving canopy regrowth could result in a stronger link between spectral recovery and forest recovery relative to what we observed in forests impacted by high severity wildfire.

Opportunities for future research are apparent

First and foremost, future studies should field-validate spectral recovery in a variety of ecological contexts (e.g., different ecosystems or regions and across a range of burn severities) to further understand how and when to use multispectral data to predict post-fire recovery. Additionally, future studies could further investigate the potential of multispectral data to improve predictive modeling of post-fire vegetation dynamics, particularly by linking spectral signatures to the recovery of different functional groups (e.g., conifers, shrubs, and grasses). In this study, we showed that multispectral data can be used to effectively identify grass-dominated sites (Fig. 4, Fig. S2); however, we required additional data inputs to effectively predict conifer recovery. Future studies could expand on our work by involving other multispectral indices to investigate how certain indices may be more effective in parsing different patterns of post-fire recovery (e.g., conifer recovery vs. shrub regeneration, vegetation transitions vs. forest recovery). Although this was not a primary objective of this study, we provide evidence that NDVI could differentiate tree- and grass-dominated sites better than NBR (Fig. S2, Fig. 4) and that NDVI-derived spectral recovery metrics outperformed NBR-derived spectral recovery metrics when predicting % juvenile conifer, shrub, and grass (Table S2). In addition to formulating more explicit links between spectral recovery—as calculated using different indices and metrics—and field-measured post-fire vegetation dynamics, future studies could investigate how to use multispectral data to predict post-fire recovery, beyond considering annual time series trends (spectral recovery). For example, connections between remote sensing data and phenology (e.g., time of senescence and length of growing season) could aid in parsing post-fire vegetation responses.

Conclusions

Climate change and fire exclusion have driven increases in wildfire frequency and severity, consequentially decreasing forest resilience and compelling framework and policy changes in the USA. When trailing edge forests burn at a high severity, they are particularly vulnerable to failed post-fire forest recovery. We advise caution and stress the importance of accounting for ecological context when interpreting spectral recovery, as in our study, in mixed conifer forests in the Blue Mountains,

fast spectral recovery was better aligned with the post-fire response of snowbrush ceanothus than with conifer regeneration. However, we suggest that by combining multispectral data with post-fire climate data and indicators of pre-fire community composition, there may be opportunities to improve predictions of post-fire forest recovery. Improving these predictions could aid land managers in deciding where to allocate resources for climate-adaptive active reforestation projects and guide applications of emerging frameworks, such as the RAD framework.

Abbreviations

AIC	Akaike's Information Criterion
BIC	Bayes' Information Criterion
CHILI	Continuous Heat-Insolation Load Index
CWD	Cumulative water deficit
DBH	Diameter at breast height
dNBR	Difference in normalized burn ratio
HLI	Heat Load Index
IR [wavelength]	Infrared
ITSPM	Individual Tree Species Parameter Maps
MTBS	Monitoring Trends in Burn Severity
NBR	Normalized burn ratio
NDVI	Normalized Difference Vegetation Index
PFFS	Post-fire fitted slope
RANOVA	Analysis of variance adjusted for random effects
RAD	Resist-Accept-Direct
REPLANT (as in REPLANT Act)	Repairing Existing Public Land by Adding Necessary Trees
SWIR [wavelength]	Short-wave infrared
TE	Trailing edge
VIF	Variance inflation factor
VPD	Vapor pressure deficit

Supplementary Information

The online version contains supplementary material available at <https://doi.org/10.1186/s42408-024-00288-6>.

Supplementary Material 1: Table S1. Replicating Table 3, with NDVI-derived spectral recovery metrics. Three generalized linear mixed effects model selections using: (1) climate and topography metrics, (2) spectral recovery metrics, and (3) all predictors. The third model selection (3) included all predictors shown in selections (1) and (2); however, predictors indicated with an asterisk in (1) or (2) were not selected for in (3); therefore, they were omitted from that portion of the table. Bolded text indicates the top-performing models out of all three model selections. Coefficients for variables selected in the top-performing model are displayed along with their significance (Kenward-Roger p -value; * $0.05 > P > 0.01$, ** $0.01 \geq P > 0.001$, *** $P \leq 0.001$), while empty cells indicate that the predictor was not selected for in the model selection. Model family, zero inflation terms (if applicable), interaction terms, AIC, BIC, and Nakagawa's marginal and conditional R^2 are all displayed. For interaction terms and zero inflation terms, the following terms were abbreviated as shown: continuous heat-insolation load index (CHILI), post-fire precipitation (Precip.), post-fire temperature (Temp.), elevation (Elev.), relative regrowth (R.R.), post-fire fitted slope (PFFS), and pre-fire canopy cover (C.C.). Table S2. Generalized linear mixed effects model results for maximal models (i.e., all spectral recovery metrics included) for (1) NBR-derived spectral recovery metrics and (2) NDVI-derived spectral recovery metrics and for (3) top-performing models identified in a model selection including both NBR- and NDVI-derived spectral recovery metrics and burn severity (dNBR) as predictors. Coefficients for variables selected in the top-performing model are displayed along with their significance (Kenward-Roger p -value; * $0.05 >$

$P > 0.01$, $**0.01 \geq P > 0.001$, $***P \leq 0.001$), while empty cells indicate that the predictor was not selected for in the model selection (for (3)). Model family, zero inflation terms (if applicable), interaction terms, AIC, BIC, and Nakagawa's marginal and conditional R^2 are all displayed. For interaction terms and zero inflation terms, the following terms were abbreviated as shown: change in NBR (ΔNBR), NBR-derived relative regrowth ($R.R._{\text{NBR}}$), change in NDVI (ΔNDVI), NDVI-derived post-fire fitted slope ($\text{PFFS}_{\text{NDVI}}$), and NDVI-derived relative regrowth ($R.R._{\text{NDVI}}$). Table S3. The number of datapoints selected from each fire for the top-down k -means cluster analysis as grouped in the slow spectral recovery and fast spectral recovery clusters. RANOVAs and Tukey-Kramer tests determined differences in the clustering of points for each fire and are displayed so that matching letters indicate no significant difference. Fires are ordered from left to right based on the proportion of points in fast recovery vs. slow recovery. Figure S1. Baseline-adjusted normalized difference vegetation index (NDVI) over time for 'fast recovery' (dark gray; $n = 55$) and 'slow recovery' (light gray; $n = 44$) k -means clusters with asterisks indicating years which the two clusters had significant ($P < 0.01$) differences in the baseline-adjusted NDVI (a). Boxplots of NDVI-derived spectral recovery metrics (k -means cluster analysis input variables; b-e) and selected field measurements (f-i) with asterisks indicating cases when one cluster had a significantly ($P < 0.05$) higher value than the cluster without an asterisk displayed. Figure S2. Baseline-adjusted normalized difference vegetation index (NDVI) over time for three k -means clusters representing grass-dominated (tan; $n = 37$), shrub-dominated (dark green; $n = 43$), and tree-dominated (light green; $n = 19$) sites (a). Significant divergence ($P < 0.01$) between clusters is shown with letters where: 's' indicates significant differences between shrub-dominated and grass-dominated clusters and 'st' indicates significant differences between tree-dominated and grass-dominated clusters and between shrub-dominated and grass-dominated clusters (a). Boxplots of spectral recovery metrics (b-e) and field metrics (k -means cluster analysis input variables; f-i) with Tukey-Kramer results indicated with letters where, if the same letter is displayed over the k -means cluster, there is no significant ($P > 0.05$) differences between those clusters for the presented variable. Figure S3. Time series for yearly climate data (PRISM) and baseline-adjusted NBR (Landsat) for each fire with solid lines displaying how yearly averages change over time. Figure S4. RdNBR time series for top-down (a) and bottom-up (b) k -means cluster analyses, using NBR-derived spectral recovery metrics as input variables in the top-down approach and field measurements as input variables in the bottom-down approach. Figure S5. Distributions of multispectral metrics (i.e., dNBR and spectral recovery metrics; shaded blue), field metrics (shaded green), and topographic metrics (shaded tan) for 'fast spectral recovery' (dark gray) and 'slow spectral recovery' (light gray) clusters from the top-down k -means cluster analysis (see Fig. 3). Asterisks indicate significant differences between k -means clusters (RANOVA; $*0.05 > P > 0.01$, $**0.01 \geq P > 0.001$, $***P \leq 0.001$). Figure S6. NBR (baseline-adjusted) over time for trailing edge (light green) and non-trailing edge (red) sites. Boxplots of projected cumulative water deficit (CWD), 2041 to 2070; Climate NA), average CWD (1981 to 2010; Climate NA), post-fire precipitation, and post-fire temperature for non-trailing edge and trailing edge sites with asterisks (*) indicating cases when one cluster had a significantly ($P \leq 0.001$) higher value than the cluster without an asterisk displayed. Figure S7. Relationships between field measurements (green points), spectral recovery metrics (blue points) and post-fire conifer regeneration probability, as derived from spatial predictive models from Davis et al. (2023). Figure S8. Linear regressions between spectral recovery metrics (red points), post-fire climate (blue points), and continuous heat-insolation load index (CHILL; tan points) and field measurements of % grass, log-transformed regeneration density, % juvenile conifer, and % shrub.

Acknowledgements

We thank undergraduate researchers who helped conduct field research including N. Ivy, L. Vining, D. West, and I. Woltering. We thank anonymous reviewers for their feedback which improved the manuscript.

Authors' contributions

All authors have read and approved the finalized study. JVC, MCF, RAA, and AJHM made substantial contributions towards the conception of the study.

JVC, MCF, and RAA worked towards acquiring field data and multispectral data. JVC led data analyses and interpretations with significant contributions from MCF, RAA, AJHM, ATS, and MSA. JVC led writing, and all authors offered substantial feedback and revisions to various manuscript drafts.

Funding

This research was funded by the US Geological Survey Northwest Climate Adaptation Science Center (NWCASC), which is managed by the USGS National Climate Adaptation Science Center under grant and cooperative agreement number UWSC14074. The conclusions and views presented in this work are those of the authors and should not be interpreted as representative of the views or policies of USGS, nor should any commercial products mentioned in the text be misinterpreted as being endorsed by USGS or NWCASC. The research was also funded by the USDA NIFA McIntire Stennis project (1019284) and USDA NIFA postdoctoral award awarded to RAA (2022-67012-37200).

Availability of data and materials

The data and supporting code from this study are available publicly, archived on GitHub (<https://github.com/celebrezze/postfire-recovery-spectral-recov-ery.git>).

Declarations

Ethics approval and consent to participate

Not applicable.

Consent for publication

Not applicable.

Competing interests

The authors declare that they have no competing interests.

Author details

¹School of the Environment, Washington State University, PO Box 642812, Pullman, WA 99164, USA. ²School of the Environment, Washington State University, Vancouver, WA, 14204 NE Salmon Creek Ave, 98686, USA.

Received: 5 February 2024 Accepted: 26 May 2024

Published online: 13 June 2024

References

- Abatzoglou, John T., and A. Park Williams. 2016. Impact of anthropogenic climate change on wildfire across western US forests. *Proceedings of the National Academy of Sciences* 113 (42): 11770–11775. <https://doi.org/10.1073/pnas.1607171113>.
- Agee, James. 1996. *Fire ecology of PNW forests*. Washington, DC: Island Press.
- Akaike, H. 1974. A new look at the statistical model identification. *IEEE Transactions on Automatic Control* 19 (6): 716–723. <https://doi.org/10.1109/TAC.1974.1100705>.
- Anderson, Michelle D. 2001. *Ceanothus velutinus*. In *Fire effects information system*. U.S. Department of Agriculture, Forest Service, Rocky Mountain Research Station, Fire Sciences Laboratory. <https://www.fs.usda.gov/database/feis/plants/shrub/ceavel/all.html>. Accessed 13 Dec 2023.
- Andrus, Robert A., Christine A. Droske, Madeline C. Franz, Andrew T. Hudak, Leigh B. Lentile, Sarah A. Lewis, Penelope Morgan, Peter R. Robichaud, and Arjan J. H. Meddens. 2022. Spatial and temporal drivers of post-fire tree establishment and height growth in a managed forest landscape. *Fire Ecology* 18 (1): 29. <https://doi.org/10.1186/s42408-022-00153-4>.
- Baker, David J., Andrew J. Hartley, James W. Pearce-Higgins, Richard G. Jones, and Stephen G. Willis. 2017. Neglected issues in using weather and climate information in ecology and biogeography. *Diversity and Distributions* 23 (3): 329–340. <https://doi.org/10.1111/ddi.12527>.
- Behnke, R., S. Vavrus, A. Allstadt, T. Albright, W.E. Thogmartin, and V.C. Radeloff. 2016. Evaluation of downscaled, gridded climate data for the conterminous United States. *Ecological Applications* 26 (5): 1338–1351. <https://doi.org/10.1002/15-1061>.

- Binkley, Dan, Kermit Cromack, and Richard Fredriksen. 1982. Nitrogen accretion and availability in some snowbrush ecosystems. *Forest Science* 28 (4): 720–724.
- Boag, Angela E., Mark J. Ducey, Michael W. Palace, and Joel Hartter. 2020. Topography and fire legacies drive variable post-fire juvenile conifer regeneration in eastern Oregon, USA. *Forest Ecology and Management* 474 (October): 118312. <https://doi.org/10.1016/j.foreco.2020.118312>.
- Bright, Benjamin C., Andrew T. Hudak, Robert E. Kennedy, Justin D. Braaten, and Azad Henareh Khalyani. 2019. Examining post-fire vegetation recovery with Landsat time series analysis in three western North American forest types. *Fire Ecology* 15 (1): 8. <https://doi.org/10.1186/s42408-018-0021-9>.
- Brooks, Mollie, Kasper Kristensen, Koen van Benthem, Arni Magnusson, Casper Berg, Anders Nielsen, Hans Skaug, Martin Maechler, and Ben Bolker. 2017. glmmTMB: Balances speed and flexibility among packages for zero-inflated generalized linear mixed modeling. *The R Journal* 9 (2): 378–400.
- Chambers, Marin E., Paula J. Fornwalt, Sparkle L. Malone, and Mike A. Battaglia. 2016. Patterns of conifer regeneration following high severity wildfire in ponderosa pine – Dominated forests of the Colorado Front Range. *Forest Ecology and Management* 378 (October): 57–67. <https://doi.org/10.1016/j.foreco.2016.07.001>.
- Chuvieco, Emilio, Inmaculada Aguado, Javier Salas, Mariano García, Marta Yebra, and Patricia Oliva. 2020. Satellite remote sensing contributions to wildland fire science and management. *Current Forestry Reports* 6 (2): 81–96. <https://doi.org/10.1007/s40725-020-00116-5>.
- Coop, Jonathan D., Sean A. Parks, Camille S. Stevens-Rumann, Shelley D. Crausbay, Philip E. Higuera, Matthew D. Hurteau, Alan Tepley, et al. 2020. Wildfire-driven forest conversion in western North American landscapes. *BioScience* 70 (8): 659–673. <https://doi.org/10.1093/biosci/biaa061>.
- Daoud, Jamal I. 2017. Multicollinearity and regression analysis. *Journal of Physics: Conference Series* 949 (December): 012009. <https://doi.org/10.1088/1742-6596/949/1/012009>.
- Davis, Kimberley T., Solomon Z. Dobrowski, Philip E. Higuera, Zachary A. Holden, Thomas T. Veblen, Monica T. Rother, Sean A. Parks, Anna Sala, and Marco P. Maneta. 2019. Wildfires and climate change push low-elevation forests across a critical climate threshold for tree regeneration. *Proceedings of the National Academy of Sciences* 116 (13): 6193–6198. <https://doi.org/10.1073/pnas.1815107116>.
- Davis, Kimberley T., Marcos D. Robles, Kerry B. Kemp, Philip E. Higuera, Teresa Chapman, Kerry L. Metlen, Jamie L. Peeler, et al. 2023. Reduced fire severity offers near-term buffer to climate-driven declines in conifer resilience across the western United States. *Proceedings of the National Academy of Sciences* 120 (11): e2208120120. <https://doi.org/10.1073/pnas.2208120120>.
- Davis, Kimberley T., Monique Wynecoop, Mary Ann Rozance, Katherine B. Swensen, Drew S. Lyons, Charlotte Dohrn, and Meade Krosby. 2024. Centering socioecological connections to collaboratively manage post-fire vegetation shifts. *Frontiers in Ecology and the Environment* e2739. <https://doi.org/10.1002/fee.2739>.
- Dodge, Jessie M., Eva K. Strand, Andrew T. Hudak, Benjamin C. Bright, Darcy H. Hammond, and Beth A. Newingham. 2019. Short- and long-term effects of ponderosa pine fuel treatments intersected by the Egly Fire Complex, Oregon, USA. *Fire Ecology* 15 (1): 40. <https://doi.org/10.1186/s42408-019-0055-7>.
- Eidenshink, Jeff, Brian Schwind, Ken Brewer, Zhi-Liang Zhu, Brad Quayle, and Stephen Howard. 2007. A project for monitoring trends in burn severity. *Fire Ecology* 3 (1): 3–21. <https://doi.org/10.4996/fireecology.0301003>.
- Ellenwood, James R., Frank J. Krist Jr, and Sheryl A. Romero. 2015. *National individual tree species Atlas*. USDA Forest Service Forest Health Technology Enterprise Team: Fort Collins.
- Enright, Neal J., Joseph B. Fontaine, David M. J. S. Bowman, Ross A. Bradstock, and Richard J. Williams. 2015. Interval squeeze: Altered fire regimes and demographic responses interact to threaten woody species persistence as climate changes. *Frontiers in Ecology and the Environment* 13 (5): 265–272. <https://doi.org/10.1890/140231>.
- Fernández-Guisuraga, José Manuel, Paulo M. Fernandes, Reyes Tárrega, David Beltrán-Marcos, and Leonor Calvo. 2023. Vegetation recovery drivers at short-term after fire are plant community-dependent in Mediterranean burned landscapes. *Forest Ecology and Management* 539 (July): 121034. <https://doi.org/10.1016/j.foreco.2023.121034>.
- Fiore, N.M., M.L. Goulden, C.I. Czimczik, S.A. Pedron, and M.A. Tayo. 2020. Do recent NDVI trends demonstrate boreal forest decline in Alaska? *Environmental Research Letters* 15 (9): 095007. <https://doi.org/10.1088/1748-9326/ab9c4c>.
- Gorelick, Noel, Matt Hancher, Mike Dixon, Simon Ilyushchenko, David Thau, and Rebecca Moore. 2017. Google Earth Engine: Planetary-scale geospatial analysis for everyone. *Remote Sensing of Environment* 202 (December): 18–27. <https://doi.org/10.1016/j.rse.2017.06.031>.
- Hagmann, R.K., P.F. Hessburg, S.J. Prichard, N.A. Povak, P.M. Brown, P.Z. Fule, R.E. Keane, et al. 2021. Evidence for widespread changes in the structure, composition, and fire regimes of western North American forests. *Ecological Applications* 31 (8): e02431. <https://doi.org/10.1002/eap.2431>.
- Hartig, Florian. 2022. DHARMA: Residual diagnostics for hierarchical (multi-level / mixed) regression models. *R Package Version 0.4.6*. <https://CRAN.R-project.org/package=DHARMA>.
- Hessburg, Paul F., James K. Agee, and Jerry F. Franklin. 2005. Dry forests and wildland fires of the inland Northwest USA: Contrasting the landscape ecology of the pre-settlement and modern eras. *Forest Ecology and Management* 211 (1–2): 117–139. <https://doi.org/10.1016/j.foreco.2005.02.016>.
- Hessburg, Paul F., Derek J. Churchill, Andrew J. Larson, Ryan D. Haugo, Carol Miller, Thomas A. Spies, Malcolm P. North, et al. 2015. Restoring fire-prone inland pacific landscapes: Seven core principles. *Landscape Ecology* 30 (10): 1805–1835. <https://doi.org/10.1007/s10980-015-0218-0>.
- Hislop, Samuel, Simon Jones, Mariela Soto-Berelov, Andrew Skidmore, Andrew Haywood, and Trung Nguyen. 2018. Using Landsat spectral indices in time-series to assess wildfire disturbance and recovery. *Remote Sensing* 10 (3): 460. <https://doi.org/10.3390/rs10030460>.
- Kassambara, Alboukadel, and Fabian Mundt. 2020. Factoextra: Extract and visualize the results of multivariate data analyses. *R Package Version 1.0.7*. <https://CRAN.R-project.org/package=factoextra>.
- Keeley, Jon E., and Sterling C. Keeley. 1981. Post-fire regeneration of southern California chaparral. *American Journal of Botany* 68 (4): 524–530. <https://doi.org/10.1002/j.1537-2197.1981.tb07796.x>.
- Kemp, Kerry B., Philip E. Higuera, Penelope Morgan, and John T. Abatzoglou. 2019. Climate will increasingly determine post-fire tree regeneration success in low-elevation forests, Northern Rockies, USA. *Ecosphere* 10 (1): e02568. <https://doi.org/10.1002/ecs2.2568>.
- Kennedy, Robert E., Zhiqiang Yang, Warren B. Cohen, Eric Pfaff, Justin Braaten, and Peder Nelson. 2012. Spatial and temporal patterns of forest disturbance and regrowth within the area of the Northwest Forest Plan. *Remote Sensing of Environment* 122 (July): 117–133. <https://doi.org/10.1016/j.rse.2011.09.024>.
- Kennedy, Robert, Zhiqiang Yang, Noel Gorelick, Justin Braaten, Lucas Cavalcante, Warren Cohen, and Sean Healey. 2018. Implementation of the LandTrendr algorithm on google earth engine. *Remote Sensing* 10 (5): 691. <https://doi.org/10.3390/rs10050691>.
- Kiel, Nathan G., and Monica G. Turner. 2022. Where are the trees? Extent, configuration, and drivers of poor forest recovery 30 years after the 1988 Yellowstone fires. *Forest Ecology and Management* 524 (November): 120536. <https://doi.org/10.1016/j.foreco.2022.120536>.
- Kim, Jong Hae. 2019. Multicollinearity and misleading statistical results. *KoreaMed Synapse* 72 (6): 558–569. <https://doi.org/10.4097/kja.19087>.
- Korb, Julie E., Paula J. Fornwalt, and Camille S. Stevens-Rumann. 2019. What drives ponderosa pine regeneration following wildfire in the western United States? *Forest Ecology and Management* 454 (December): 117663. <https://doi.org/10.1016/j.foreco.2019.117663>.
- Lenth, Russell V. 2021. Emmeans: Estimated marginal means, aka least-squares means. *R Package Version 1.5.4*. <https://CRAN.R-project.org/package=emmeans>.
- Lotan, James E. 1976. Cone serotiny - fire relationships in lodgepole pine. In *Tall timbers fire ecology conference proceedings*.
- Luke, Steven G. 2017. Evaluating significance in linear mixed-effects models in R. *Behavior Research Methods* 49 (4): 1494–1502. <https://doi.org/10.3758/s13428-016-0809-y>.
- Meigs, Garrett W., Michael J. Case, Derek J. Churchill, Charles M. Hersey, Sean M. A. Jeronimo, L. Annie, and C. Smith. 2023. Drought, wildfire and forest transformation: Characterizing trailing edge forests in the eastern Cascade Range, Washington, USA. *Forestry* 96 (3): 340–354. <https://doi.org/10.1093/forestry/cpac046>.
- Meng, Ran, Philip E. Dennison, Chengquan Huang, Max A. Moritz, and Carla D'Antonio. 2015. Effects of fire severity and post-fire climate on short-term vegetation recovery of mixed-conifer and red fir forests in the Sierra

- Nevada Mountains of California. *Remote Sensing of Environment* 171 (December): 311–325. <https://doi.org/10.1016/j.rse.2015.10.024>.
- Nakagawa, Shinichi, and Holger Schielzeth. 2013. A general and simple method for obtaining R^2 from generalized linear mixed-effects models. *Methods in Ecology and Evolution* 4 (2): 133–142. <https://doi.org/10.1111/j.2041-210x.2012.00261.x>.
- Neath, Andrew A., and Joseph E. Cavanaugh. 2012. The Bayesian information criterion: Background, derivation, and applications. *Wires Computational Statistics* 4 (2): 199–203. <https://doi.org/10.1002/wics.199>.
- NRCS Web soil survey. 2012. <http://websoilsurvey.nrcs.usda.gov>. Accessed 23 Nov 2023.
- Park, Isaac W., and G. Darrel Jenerette. 2019. Causes and feedbacks to widespread grass invasion into chaparral shrub dominated landscapes. *Landscape Ecology* 34 (3): 459–471. <https://doi.org/10.1007/s10980-019-00800-3>.
- Parks, S.A., and J.T. Abatzoglou. 2020. Warmer and drier fire seasons contribute to increases in area burned at high severity in western US forests from 1985 to 2017. *Geophysical Research Letters* 47 (22): e2020GL089858. <https://doi.org/10.1029/2020GL089858>.
- Parks, Sean A., Lisa M. Holsinger, Matthew H. Panunto, W. Matt Jolly, Solomon Z. Dobrowski, and Gregory K. Dillon. 2018. High-severity fire: Evaluating its key drivers and mapping its probability across western US forests. *Environmental Research Letters* 13 (4): 044037. <https://doi.org/10.1088/1748-9326/aab791>.
- Parks, Sean A., Solomon Z. Dobrowski, John D. Shaw, and Carol Miller. 2019. Living on the edge: Trailing edge forests at risk of fire-facilitated conversion to non-forest. *Ecosphere* 10 (3): e02651. <https://doi.org/10.1002/ecs2.2651>.
- Pausas, Juli G. 2015. Bark thickness and fire regime. *Functional Ecology* 29 (3): 315–327. <https://doi.org/10.1111/1365-2435.12372>.
- Pearce, David W. 2001. The economic value of forest ecosystems. *Ecosystem Health* 7 (4): 284–296. <https://doi.org/10.1046/j.1526-0992.2001.01037.x>.
- Pérez-Cabello, Fernando, Raquel Montorio, and Daniel Borini Alves. 2021. Remote sensing techniques to assess post-fire vegetation recovery. *Current Opinion in Environmental Science & Health* 21 (June): 100251. <https://doi.org/10.1016/j.coesh.2021.100251>.
- Pickell, Paul D., Txomin Hermosilla, Ryan J. Frazier, Nicholas C. Coops, and Michael A. Wulder. 2016. Forest recovery trends derived from Landsat time series for north American boreal forests. *International Journal of Remote Sensing* 37 (1): 138–149. <https://doi.org/10.1080/2150704X.2015.1126375>.
- PRISM Climate Group, Oregon State University. 2014. <https://prism.oregonstate.edu>. Accessed 1 Oct 2023.
- Repairing Existing Public Land by Adding Necessary Trees Act within the Infrastructure Investment and Jobs Act, Pub. L. No. 117-58. 2021. Accessed 18 Nov 2023.
- Rodman, Kyle C., Joseph E. Crouse, Jonathon J. Donager, David W. Huffman, and Andrew J. Sánchez-Meador. 2022. Patterns and drivers of recent land cover change on two trailing-edge forest landscapes. *Forest Ecology and Management* 521 (October): 120449. <https://doi.org/10.1016/j.foreco.2022.120449>.
- Rollins, Matthew G. 2009. LANDFIRE: A nationally consistent vegetation, wild-land fire, and fuel assessment. *International Journal of Wildland Fire* 18 (3): 235. <https://doi.org/10.1071/WF08088>.
- Rother, Monica T., and Thomas T. Veblen. 2016. Limited conifer regeneration following wildfires in dry ponderosa pine forests of the Colorado Front Range. *Ecosphere* 7 (12): e01594. <https://doi.org/10.1002/ecs2.1594>.
- Schuurman, Gregor W., David N. Cole, Amanda E. Cravens, Scott Covington, Shelley D. Crausbay, Cat Hawkins Hoffman, David J. Lawrence, et al. 2022. Navigating ecological transformation: Resist–accept–direct as a path to a new resource management paradigm. *BioScience* 72 (1): 16–29. <https://doi.org/10.1093/biosci/biab067>.
- Schuurman, Gregor, Hawkins-Hoffman Cat, David Cole, David Lawrence, John Morton, Dawn Magness, Amanda Cravens, Scott Covington, Robin O'Malley, and Nicholas Fischeilli. 2020. *Resist-Accept-Direct (RAD)—A framework for the 21st-century natural resource manager*. National Park Service. <https://doi.org/10.36967/nrr-2283597>.
- Smith-Tripp, Sarah M., Nicholas C. Coops, Christopher Mulverhill, Joanne C. White, and Jodi Axelson. 2024. Landsat assessment of variable spectral recovery linked to post-fire forest structure in dry sub-boreal forests. *ISPRS Journal of Photogrammetry and Remote Sensing* 208 (February): 121–135. <https://doi.org/10.1016/j.isprsjprs.2024.01.008>.
- Soulard, Christopher E. 2012. Blue Mountains ecoregion. In *Status and trends of land change in the western United States—1973 to 2000: U.S. geological survey professional paper*, ed. Benjamin Sleeter, Tamara Wilson, and William Acevedo, 169–177.
- Steinley, Douglas. 2006. K-means clustering: A half-century synthesis. *British Journal of Mathematical and Statistical Psychology* 59 (1): 1–34. <https://doi.org/10.1348/000711005X48266>.
- Stevens-Rumann, Camille S., Kerry B. Kemp, Philip E. Higuera, Brian J. Harvey, Monica T. Rother, Daniel C. Donato, Penelope Morgan, and Thomas T. Veblen. 2018. Evidence for declining forest resilience to wildfires under climate change. *Ecology Letters* 21 (2): 243–252. <https://doi.org/10.1111/ele.12889>.
- Stevens-Rumann, Camille S., Susan J. Prichard, Ellen Whitman, Marc-André. Parisien, and Arjan J.H.. Meddens. 2022. Considering regeneration failure in the context of changing climate and disturbance regimes in western North America. *Canadian Journal of Forest Research* 52 (10): 1281–1302. <https://doi.org/10.1139/cjfr-2022-0054>.
- Stine, Peter, Paul Hessburg, Thomas Spies, Marc Kramer, Christopher J. Fettig, Andrew Hansen, John Lehmkuhl, et al. 2014. *The ecology and management of moist mixed-conifer forests in eastern Oregon and Washington: A synthesis of the relevant biophysical science and implications for future land management*. PNW-GTR-897. Portland: U.S. Department of Agriculture, Forest Service, Pacific Northwest Research Station. <https://doi.org/10.2737/PNW-GTR-897>.
- Storey, Emanuel A., Douglas A. Stow, and John F. O'Leary. 2016. Assessing postfire recovery of chamise chaparral using multi-temporal spectral vegetation index trajectories derived from Landsat imagery. *Remote Sensing of Environment* 183 (September): 53–64. <https://doi.org/10.1016/j.rse.2016.05.018>.
- Theobald, David M., Dylan Harrison-Atlas, William B. Monahan, and Christine M. Albano. 2015. Ecologically-relevant maps of landforms and physiographic diversity for climate adaptation planning. *PLoS One* 10 (12): e0143619. <https://doi.org/10.1371/journal.pone.0143619>.
- Thompson, Ian D., Kimiko Okabe, Jason M. Tyliranakis, Pushpam Kumar, Eckehard G. Brockerhoff, Nancy A. Schellhorn, John A. Parrotta, and Robert Nasi. 2011. Forest biodiversity and the delivery of ecosystem goods and services: Translating science into policy. *BioScience* 61 (12): 972–981. <https://doi.org/10.1525/bio.2011.61.12.7>.
- Timberlake, Thomas J., and Courtney A. Schultz. 2019. Climate change vulnerability assessment for forest management: The case of the U.S. forest service. *Forests* 10 (11): 1030. <https://doi.org/10.3390/f10111030>.
- Vanderhoof, Melanie K., Todd J. Hawbaker, Ku. Andrea, Kyle Merriam, Erin Berryman, and Megan Cattau. 2021. Tracking rates of postfire conifer regeneration vs. deciduous vegetation recovery across the western United States. *Ecological Applications* 31 (2): e02237. <https://doi.org/10.1002/eap.2237>.
- Viana-Soto, Alba, Inmaculada Aguado, Javier Salas, and Mariano García. 2020. Identifying post-fire recovery trajectories and driving factors using Landsat time series in fire-prone Mediterranean pine forests. *Remote Sensing* 12 (9): 1499. <https://doi.org/10.3390/rs12091499>.
- Wang, Tongli, Andreas Hamann, Dave Spittlehouse, and Carlos Carroll. 2016. Locally downscaled and spatially customizable climate data for historical and future periods for North America. *PLoS One* 11: e0156720. <https://doi.org/10.1371/journal.pone.0156720>.
- White, Joanne C., Michael A. Wulder, Txomin Hermosilla, Nicholas C. Coops, and Geordie W. Hobart. 2017. A nationwide annual characterization of 25 years of forest disturbance and recovery for Canada using Landsat time series. *Remote Sensing of Environment* 194 (June): 303–321. <https://doi.org/10.1016/j.rse.2017.03.035>.
- White, Joanne C., Txomin Hermosilla, and Michael A. Wulder. 2023. Pre-fire measures of boreal forest structure and composition inform interpretation of post-fire spectral recovery rates. *Forest Ecology and Management* 537 (June): 120948. <https://doi.org/10.1016/j.foreco.2023.120948>.
- Williams, A. Park., and John T. Abatzoglou. 2016. Recent advances and remaining uncertainties in resolving past and future climate effects on global fire activity. *Current Climate Change Reports* 2 (1): 1–14. <https://doi.org/10.1007/s40641-016-0031-0>.
- Yang, Jia, Shufen Pan, Shree Dungal, Bowen Zhang, Siyuan Wang, and Hanqin Tian. 2017. Continental-scale quantification of post-fire vegetation greenness recovery in temperate and boreal North America. *Remote Sensing*

of Environment 199 (September): 277–290. <https://doi.org/10.1016/j.jrse.2017.07.022>.

Zuur, Alain F., Elena N. Ieno, Neil Walker, Anatoly A. Saveliev, and Graham M. Smith. 2009. *Mixed effects models and extensions in ecology with R. Statistics for biology and health*. New York: Springer New York. <https://doi.org/10.1007/978-0-387-87458-6>.

Publisher's Note

Springer Nature remains neutral with regard to jurisdictional claims in published maps and institutional affiliations.